NUMERICAL SIMULATION AND EXPERIMENTAL VALIDATION OF THE RE-DESIGN OF HIGH T$_C$ CURRENT LEADS FOR THE ASTRO-E2 X-RAY SPECTROMETER DETECTOR SYSTEM

By

Victor L. Marrero Ortiz

A thesis submitted in partial fulfillment of the requirements for the degree of

MASTER OF SCIENCE

in

MECHANICAL ENGINEERING
(Thermal Science)

UNIVERSITY OF PUERTO RICO
MAYAGUEZ CAMPUS

December 2003

Approved by:

_____   _____
Nellore S. Venkataraman, Ph.D.   Date
Member, Graduate Committee

_____   _____
Gustavo Gutiérrez, Ph.D.   Date
Member, Graduate Committee

_____   _____
Sandra Coutín Rodicio, Ph.D.   Date
President, Graduate Committee

_____   _____
José A. Vega, Ph.D.   Date
Representative of Graduate Studies

_____   _____
Paul A. Sundaram, Ph.D.   Date
Chairperson of the Department

ABSTRACT

The herein presented research work consists on the redesign and thermal model development of the X-Ray Spectrometer (XRS) High T_c Superconducting Current (HTSC) lead assembly. The HTSC leads are used to provide current to the Adiabatic Demagnetization Refrigerator (ADR), which is used for cooling the XRS instrument to a 60 mK platform. The XRS is intended to study X-Rays emitted by astronomical objects, such as black holes, to determine their X-Ray spectrum. In order to achieve a 2.5-year lifetime goal for the XRS it is necessary to developed low thermal conductance leads to supply current to the ADR magnet and the cryostat valve motors with a minimal heat load. Superconducting Magnesium Diboride (MgB_2) wires, with 39 K superconductivity, are used to conduct current from the 17 K support structure to the 4 K vapor cooled stage. Nobidium Titanium (NbTi) wires are used to provide a superconducting path from the 4 K stage to the magnet and valves on the 1.3 K Helium cryostat. This research investigation aimed to develop a prototype of the HTSC lead assembly and a computer model to simulate the thermal behavior of this system. Experimental data from the prototype was used to validate the thermal model, which was employed to minimize heat loads in the design.

RESUMEN

El objetivo de esta investigación es el rediseño y desarollo de un modelo termal de los cables Superconductores de Corriente de Alta Temperatura Crítica (HTSC) para un Espectrómetro de Rayos X (XRS). Los cables HTSC son usados para proveer corriente eléctrica al Refrigerador Adiabático de Demagnetización (ADR), que se usa para enfriar el instrumento XRS a una temperatura estable de 60 mK. El XRS ha sido diseñando para estudiar los rayos X emitidos por objetos astronómicos, como agujeros negros, para determinar sus espectros de rayos X. Para alcanzar la meta de una vida de 2.5 años para el XRS, fue necesario desarollar unos cables de baja conducción térmica para proveer corriente al magneto del ADR y a los motores de unas válvulas criogénicas con la mínima cantidad de calor. Cables del superconductor diboro de magnesio (MgB$_2$), con una superconductividad a 39 K, fueron usados para proveer corriente desde una estructura a 17 K hasta una estación enfriada por vapor a 4 K. Cables de Nobidio de Titanio (NbTi) fueron usados para proveer la corriente de la estación de 4 K hasta el magneto y las válvulas en el tanque de Helio a 1.3 K. Esta investigación consiste en el desarrollo de un prototipo de los cables HTSC y el desarrollo de un modelo en computadora para simular el comportamiento térmico del sistema. Datos experimentales se usaron para validar el modelo térmico, el cual fue usado para minimizar la carga de calor en el diseño.

DEDICATION

To my parents, Victor L. Marrero and Edith V. Ortiz, for providing me the significance of higher education as well as the importance of hard work. Without their unconditional support this work would have not been successful.

ACKNOWLEDGMENTS

TABLE OF CONTENT

LIST OF TABLES

LIST OF FIGURES

NOMENCLATURE

A_c	Cross sectional area (m^2)
ADR	Adiabatic Demagnetization Refrigerator
CICC	Cable-in-Conduit Conductor
CGRO	Compton Gamma Ray Observatory
Cu	Copper
C_v	Specific Heat (kJ/kg·K)
dx	Finite length (m)
EXOSAT	European X-ray Observatory Satellite
GSFC	Goddard Space Flight Center
h	Planck's constant (J·s)
He	Helium
HEAO	High Energy Astrophysical Observatory
HTSC	High Temperature Superconducting Current
HTS	High Temperature Superconductor
HXD	Hard X-ray detector
ISAS	Institute of Space and Astronautical Science
K	Boltzmann's constant (J/K)
K_T	Thermal conductivity integral (W/m)
k	Thermal conductivity (W/m·K)
LHe	Liquid Helium

MgB$_2$	Magnesium Diboride
NASA	National Aeronautics and Space Administration
NbTi	Nobidium Titanium
Ne	Neon
PIT	Powder-in-Tube
PTFE	Polytetrafluoroethylene
Q_c	Total heat flow (W)
q_x	Heat flux per unit area (W/m^2)
$\Re$	Universal gas constant (kJ/kgmol·K)
ROSAT	Röntgen Satellite
SS316	Stainless Steel 316
TAO	Thermoacoustic Oscillation
T	Temperature (K)
V	Volume (m^3)
XIS	X-ray Imaging Spectrometer
XRS	X-ray Spectrometer
YBCO	YBaCuO

Greek Symbols

ε	Emissivity (dimensionless)
v_E	Single frequency of vibration (1/s)
v_m	Maximum frequency of vibration (1/s)

θ_E Einstein characteristic temperature (K)

θ_D Debye characteristic temperature (K)

σ Stefan-Boltzmann constant ($W/m^2 \cdot K^4$)

CHAPTER 1

INTRODUCTION

1.1 BACKGROUND

The continuous interest in understanding the Universe have inspired and motivated scientists and engineers at the National Aeronautics and Space Administration (NASA) to develop various devices to gain unique and significant information. These efforts lead to answer questions such as "How did the Universe begin and how does it evolve?". One approach to address these questions is to study X-rays emitted by astronomical objects such as black holes, galactic centers, and births and deaths of stars.

High energetic X-rays can penetrate the air at least at distances of a few meters. However, the Earth's atmosphere is thick enough that basically most of the X-rays emitted by astronomical objects are unable to penetrate from outer space all the way to the Earth's surface. Most astronomical objects give off the bulk of their energy on the low X-ray energetic range which can be stopped by a few sheets of paper. Therefore, in order to observe X-rays from astronomical objects, X-ray detectors must be flown above most of the Earth's atmosphere. At the present there are three possible methods: Rockets, Balloons and Satellites. Nowadays, most of the studies of high-energy astrophysics are carried out using data from a host of satellites such as: the HEAO series, EXOSAT, CGRO, and ROSAT. Data from these satellites, contribute to the understanding of the nature of these sources and the mechanisms by which the X-rays are emitted, leading to a

better understanding of fundamental physics of our universe. In recent years, NASA and other institutions have been developing new astronomical X-rays observatories such as ASTRO-E2 and future Constellation-X.

ASTRO-E2 is a recovery mission, approved after the lost during launch of ASTRO-E in February 2000. ASTRO-E was meant to be Japan's fifth X-ray Astronomy mission, and was developed at the Institute of Space and Astronautical Science (ISAS) in Japan, in collaboration with the United States. ASTRO-E2 is a virtual replica of the original mission with three instruments aboard: X-ray CCDs (X-ray Imaging Spectrometer; XIS), the Hard X-ray detector (HXD) and X-ray micro-calorimeter (X-ray Spectrometer; XRS). The XRS is a high resolution X-ray instrument aboard the ASTRO-E2 satellite which consists of an array of 32 calorimeters, each capable of detecting X-rays in the energy range of 0.3-10 keV with a resolution of 12 eV. The calorimeters are sensors which measure heat input. These calorimeters measure the energy of X-ray photons by measuring the heat energy deposited when the photons are absorbed. In order to be able to reach high resolution, the XRS detectors are cooled to 60 mK using a cryogenic system of solid neon, superfluid helium and an Adiabatic Demagnetization Refrigerator (ADR).

The ASTRO-E2 XRS will be the first X-ray microcalorimeter to fly on an orbiting observatory. It is scheduled to be launched on February 2005 and be on orbit for 2-years with approximate 20 liters of superfluid helium. In order to meet the lifetime requirement, the total heat load to the superfluid helium must be less that 1 mW, which is significantly smaller than previous spaceborne helium systems.

Figure 1.1 shows different components during the original XRS/Cryostat Flight Assembly. At the bottom of the figure the He fill and vent lines are shown and on the left is the High Temperature Superconducting Current (HTSC) leads which conducts the current to the ADR magnet and to the cryostat valves.
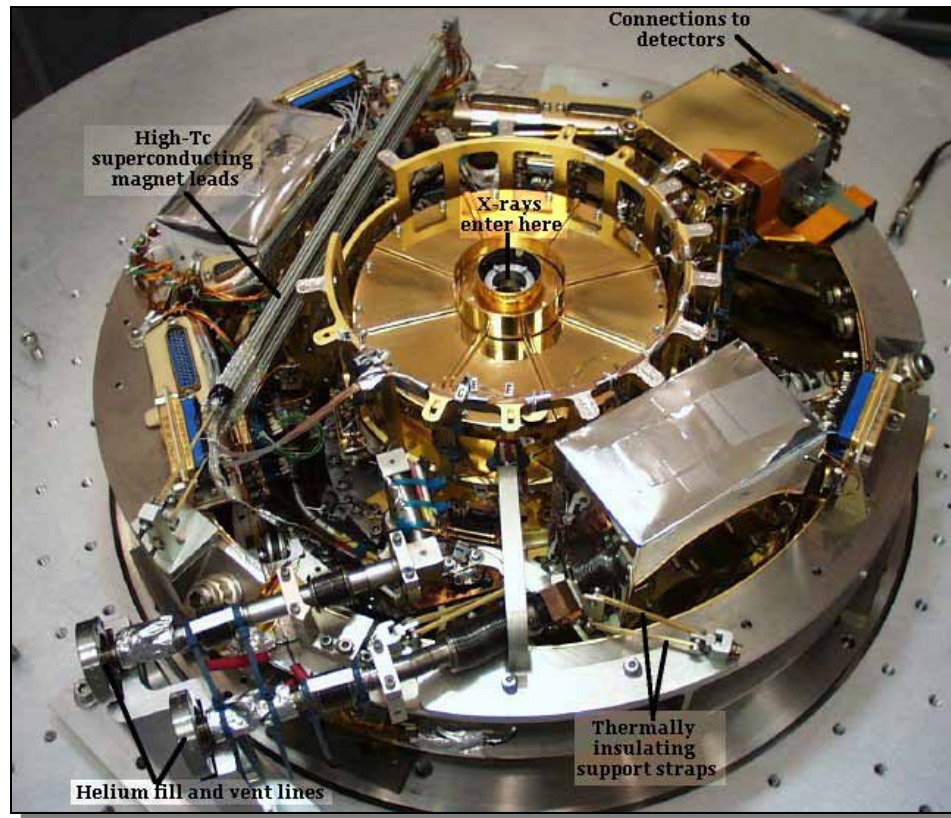
Figure 1.1. Top View of the XRS flight He Insert During Assembly

1.2 ADIABATIC DEMAGNETIZATION REFRIGERATOR (ADR)

In the late 1920's it was suggested by Giauque (1927) and Debye (1926) a suitably disordered system to be an assembly of magnetic dipoles. It was understood that the energy scale of the interaction of typical magnetic moments in insulating paramagnetic materials with the magnetic fields was in the neighborhood of liquid helium

(LHe) temperatures.   Thus, through isothermal magnetization and adiabatic demagnetization, cooling might be achieved.

NASA Goddard Space Flight Center (GSFC) began working on the first space-based ADR in 1979. The ADR developed by GSFC was a heat pump that operated between liquid helium (LHe) temperature (~1.3 K) and very low temperatures (~60 mK). This technology is used to provide a stable 60 mK platform to the XRS detector in order to obtain high resolution. An ADR was chosen for outer space instead of a dilution refrigerator because it does not require gravity and because it is exceedingly efficient.

The ADR for the XRS has an efficiency of approximately 50% Carnot's. This efficiency is necessary for space-based systems to allow the LHe storage tank, herein called dewar or cryostat, to operate for extended periods of time on orbit. The ADR does not run continuously, it stores the heat that is absorbed from the calorimeters and the heat that is leaked. The ADR consists of different components as shown in Figure 1.2.

The heat coming from the calorimeters is transferred to the ADR through gold-plated copper rods called thermal bus. Then, the heat is transfer to the paramagnetic salt pill where the cooling takes place. The heat is then stored in the salt pill, made of a ferric ammonium sulfate. The horizontal lines running through the salt pill represent gold wires that provide good thermal contact from the salt pill material to the heat switch and thermal busses.
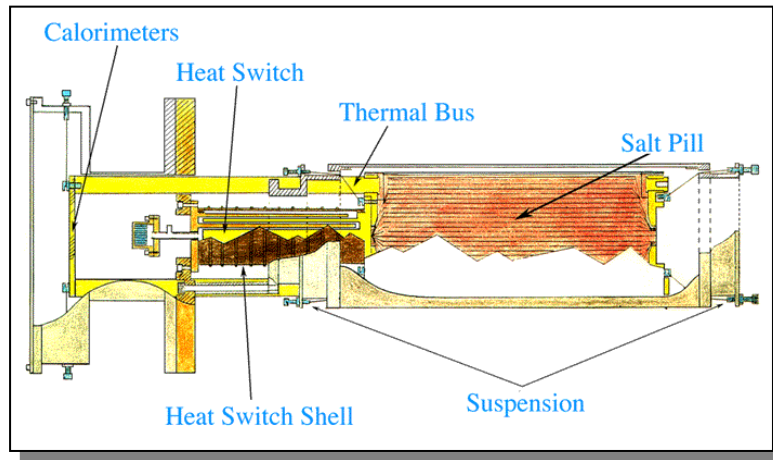
Figure 1.2. Adiabatic Demagnetization Refrigerator Diagram

The outer structure of the ADR consists of metal rings and tubes, which allow the ADR to fit securely within the superconducting magnet (not shown). The salt pill is suspended within this rigid outer structure by means of Kevlar cords which are strong enough to hold the salt pill in place during the stress in launching. The Kevlar has low thermal conductivity such that not much heat leaks into the salt pill through the suspension. When in use, the salt pill end of the ADR is slid into a superconducting magnet. Changing the applied magnetic field causes the salt pill to cool and conduct away the heat to the LHe bath (not shown), through the heat switch. This process decreases the entropy of the salt pill isothermally. The heat switch is then opened and the magnetic field is reduced, causing the salt pill to demagnetize adiabatically, and the system cools down, as shown in Figure 1.3.

The XRS cryostat serves mainly as a 1.3 K heat sink for the ADR and associated wiring. The heat load requirement for meeting a 2.5-year lifetime goal is approximately 1.0 mW. In order to achieve this low value it was necessary to develop low thermal

conductance leads to supply current to the ADR magnet and the cryostat valve motors, with a minimal heat load [1]. The use of High T_c Superconducting material, which is discussed in details in the next section, is needed to satisfy the basic thermal and electrical requirements to meet the 2.5-year lifetime.
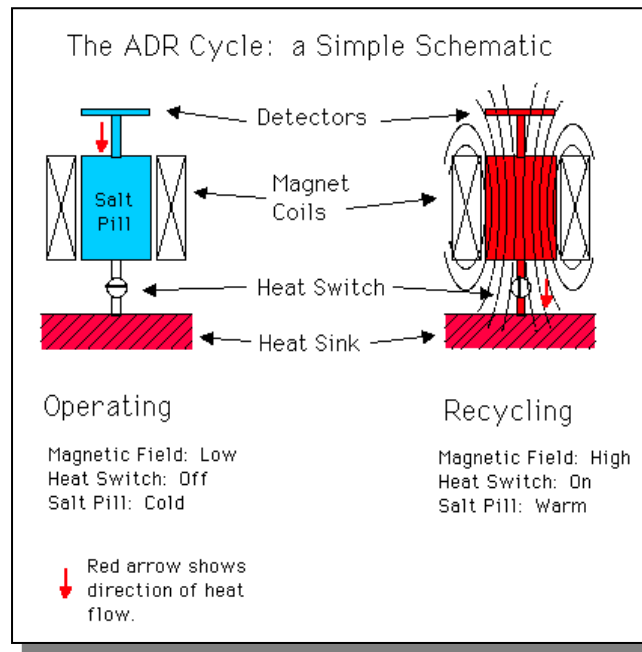
Figure 1.3. ADR Cycle Diagram

1.3 HIGH TEMPERATURE SUPERCONDUCTING CURRENT (HTSC) LEADS

In order to increase the orbiting lifetime for the XRS it was necessary to develop low thermal conductance leads to supply electric current to the ADR magnet with a minimal heat load. The XRS HTSC leads consist of an assembly of superconducting material developed to conduct current from a 17 K temperature stage to a 1.3 K temperature stage. The operation of the cryostat valve motors, which operates on ground only, and the ADR magnet requires wiring with sufficiently large diameter to safely

handle the drive current up to 2 amps. On other hand, the wire diameter must be as small as possible to minimize heat loads into the LHe cryostat. A vapor Helium (He) vent line, which under normal operating conditions operates at less than 4 K, is available to intercept some of the conducted heat. Since the XRS dewar has such a small volume of LHe, in order to meet the lifetime requirement of 2.5-years, the heat loads to the helium tank must be maintained below 1.0 mW.

The use of High Temperature Superconductor (HTS) material in the HTSC leads is advantageous because it has the potential to reduce the refrigeration requirements to significantly low values compared to conventional leads. The need for low heat load eliminates the possibility of using copper wires for the HTSC leads. The heat load from copper leads was 2.7 milliwatts, when the leads were optimized for the best tradeoff between Joule heating and heat conduction [1]. Low temperature superconductors, such as NbTi cannot be used. This is because the "warm" end temperature of 17 K which is above its superconducting transition temperature of 9 K. This means that when the superconducting material reaches this temperature, it is not superconducting anymore. It losses the capability of conducting electric current in a virtual non-resistance environment. Above the transition temperature, the Joule heating plays an important role in determining the capacity of the material to conduct current without burning. A hybrid lead, with the "cold" component of NbTi and the "warm" component of copper is likewise unworkable. Joule heating of the copper would warm the NbTi above its transition temperature, even if the lead were cooled through a heat sink to the helium vapor vent line [1]. The XRS cryostat design team at NASA decided to use high

temperature superconductors for the high current leads. The combined high electrical conductivity and low thermal conductivity will hold down both Joule heating and thermal conduction.

The original XRS HTSC leads design consisted of an assembly of superconducting YBaCuO (YBCO) fibers bonded to a fiberglass tube and suspended by a Kevlar suspension string for isolation. It was developed to conduct current from the 17 K support structure to the 4 K vapor cooled stage, as shown in Figure 1.4.
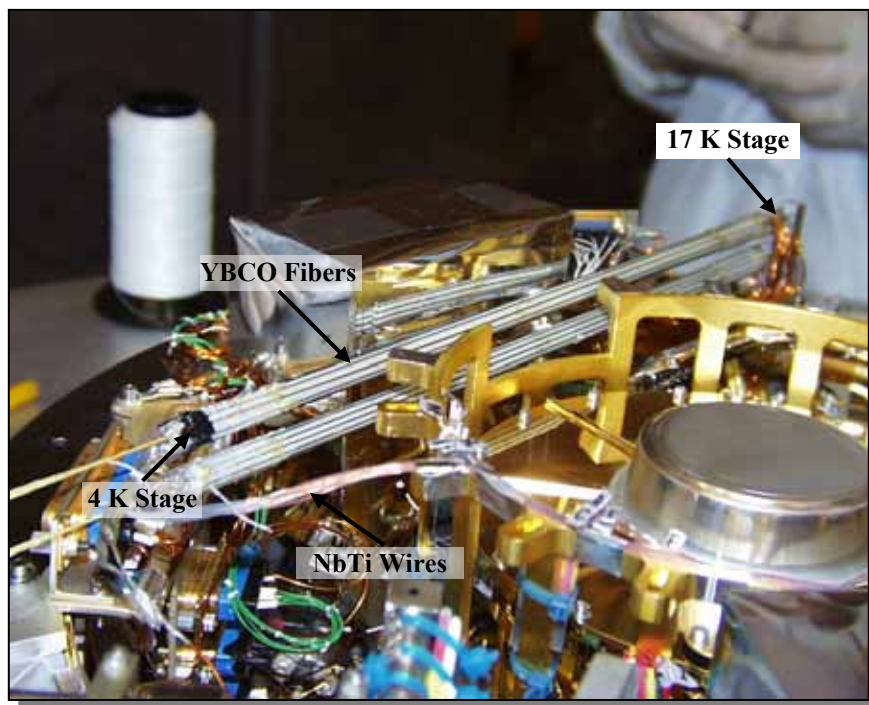
Figure 1.4. XRS HTSC Leads Flight Assembly

Superconducting NbTi wire, which has a critical temperature of 9 K, was used to conduct the current from the 4 K stage to the ADR magnet and cryostat valves on the 1.3 K LHe tank, as shown in Figure 1.5 [1].
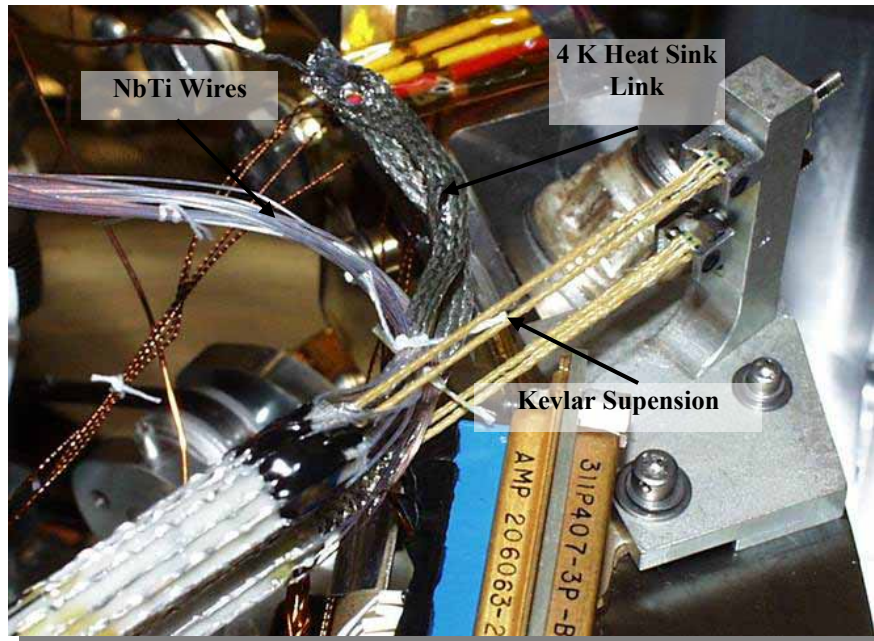
Figure 1.5. YBCO/NbTi Interface and 4 K Heat Sink

If for any reason the temperature of the NbTi wire reaches 9 K while carrying current, the increased electrical resistance could cause the wire to burn out. Verifications were made during tests of the cryostat and He insert to assured that the NbTi leads remained superconducting under the expected thermal conditions, including the brief loss of vapor-cooling of the vent line during cryogen servicing operations [2].

1.4 RESEARCH PROBLEM

In the original XRS the HTSC leads assembly performed well under nominal conditions. However, one of the problems faced by the engineers at NASA was the assembly failure in two occasions when exposed to radiation from high-temperature sources. The radiation causes the NbTi wires to heat up to 9 K, superconducting

transition temperature, and burn out [3]. Additionally, it was encountered that after the integration with the Neon (Ne) Dewar a particular valve configuration between the LHe fill line and the He cooling loops on the Ne tank caused thermoacoustic oscillations (TAOs) in the He Dewar vent line. These oscillations caused the vent line heat sink to briefly exceed 9 K. The procedural steps that led to this valve configuration were modified to prevent this from reoccurring [4].

Based on these events, the HTSC assembly was classified to be the most programmatic risk of failure in the XRS project. If HTSC assembly failed, the ADR will not have the electric current needed to cool the XRS detector to the design temperature and, as a result the entire mission will fail. Based on theses experience, a new design for the HTSC leads was proposed, where the heat sink will provide a better range of safety for the entire mission.

1.5 RESEARCH GOALS

The main goal of the herein research work is to redesign the original ASTRO-E HTSC leads to provide a better margin of safety to the entire mission. The design parameter of this research is mainly focus to the thermal performance of the HTSC leads, specially the amount of heat conducted along the system.   The specific steps involved in this research are as follows:

1. Development of a prototype.

2. Design and calibration of the experimentation environment.

3. Thermal performance tests of the prototype.

4. Development of a thermal computer model to describe the thermal behavior of the HTC leads.

5. Validation of the computer model with experimental data.

6. Development of the final assembly.

The thermal model developed in this investigation has unique characteristics. The model is a one-dimensional conduction and radiation heat transfer model, which considers a temperature dependent thermal conductivity and a variable emissivity of the material. The experimental data is used to validate the model. A complete development and validation of the model is included in Chapters 4 and 5, respectively.

1.5.1 EXPERIMENTATION

The experimentation of the new XRS HTSC was conducted at the Cryogenics and Fluids Branch laboratory facilities at NASA GSFC. A Janis Research Inc. 19" Cryogenics Dewar was used to conduct a thermal performance test in vacuum for the prototype and final assembly. The thermal performance test is focus mainly in measured the amount of heat conducted through the system rather than measured the temperature distribution along the system. The prototype development and the final XRS-2 HTSC assembly construction and thermal experimentation setup are discussed in detail in Chapter 3. Experimental results and validation of a computer model is presented in detail in Chapter 5.

1.5.2   MODELING

The HTSC assembly plays an important role in determining the life-time for the entire mission. A good thermal model that can predict the thermal performance of the HTSC leads will be a useful tool in different ways. The model can be used as a design tool for future HTSC leads like the next orbit X-Ray observatory Constellation-X. Engineers can use the model at early stages of the design to make important decisions on the type of materials needed and the type of configurations to meet the design requirements.

The model can be also used after the design is finished and fully operational. It has applications in determining the direct impact of the assembly to the total life-time of the spacecraft. This is very useful in the flight planning in case that for any reason the operating conditions of the spacecraft change while in orbit. By running the model with the new environment conditions, it can help scientists and engineers to calculate the new life-time of the spacecraft and make the necessary adjustments to mission objectives.

CHAPTER 2

LITERATURE REVIEW

The main objective of a good HTSC lead design is to minimize the heat leak introduced by the transmission of a given current into the cryostat system. In most cryogenic systems, this heat comes from three different sources. The first source is the heat conducted down through the lead, because of the difference in temperature along the leads. The second source is the heat generated within the lead by ohmic loss called Joule heating. The third source is the heat that reached the leads by radiation from another body. In the design phase, it is more feasible to control the first two heat sources. Hence, for a good HTSC design it is desirable to minimize both: heat conduction and the electrical resistance.

In 1911 Heike Kammerlingh Onnes discovered the superconductivity while searching for zero electrical resistance in Mercury [5]. Thereafter, as a major research area in Applied Physics, a lot of efforts by researchers have been made in the development and understanding of the utilization of superconductivity in many applications. In HTSC leads, zero electrical resistance means that there is no Joule heating in the wire and therefore it can carry a higher current density. This is an advantage, because it can be packed closely together without much worry about heat removal. One of the major applications of superconductivity is the construction of superconducting magnets that can provide high magnetic fields.

Superconducting magnets are usually energized at LHe temperature by the HTSC leads assembly that comes from a power source at room temperature. The temperature gradient and Joule heating in the HTSC leads are usually the dominant source of parasitic heat leaking into the magnet cryostat. The magnet cryostat is the enclosure where the LHe is located and it is the parasitic heat leak which largely determines the running cost of the magnet system in terms of LHe consumption. Therefore, it is important to ensure that in the design the available cooling capacity of the LHe is utilized as fully as possible, not only the latent heat of vaporization, but also the change in enthalpy of the gas as it warms up to room temperature. For example, a heat leak of 1 Joules will vaporize 48 mg of LHe, but an additional amount of 74 Joules will be required to warm up this mass of gas up to room temperature [5]. In the XRS detector system a vapor He vent line, which under normal operating conditions operates at 4 K, is available to intercept some of the conducted heat from the HTSC.

In practice, it is very difficult to design HTSC leads because in most cases the temperature dependent resistivity and thermal conductivity of a given piece of metal are rarely known over the whole operating temperature range. Therefore, the HTSC leads should be redesigned thoroughly and as best as possible with the data available and, tested experimentally until the design is optimal.

Nowadays technology employs computer models as an important part of the design since it is a practical tool which helps to decrease the design cost and time. In many HTSC leads designs, understanding the thermal stability of the leads assembly is an important task. Computer models capable of accurately calculating the temperature

distribution along the HTSC leads, under operating conditions, will allow researchers to better design HTSC leads, for any given application.

Many research efforts have been made during the last decades in developing general HTSC modeling tools to optimize and reduce the design time. Thermal modeling of HTSC has been focused on identifying the temperature distribution and amount of heat through the system and it has been used as a tool to optimize the design. It has mostly been used to understand the burnout of the leads caused by Joule heating and thermal disturbances.

The simple case of modeling an HTSC lead is considering the leads system as a one-dimensional conduction model. Many authors employed a one-dimensional transient conduction model to study the burnout time and critical energy in a HTSC caused by Joule heating [6, 7]. Seol et al. [6] and Malinowski [7] considered the HTSC leads cooling by conduction only. Seol et al. considered the thermophysical properties temperature dependence, while Malinowski considered these properties as constant. The consideration of constant or variable properties depends strongly on the type of HTSC lead material used and the temperature range in which the system is being modeled. These models by Seol et al [6] and Malinowski [7] predict a fair approximation of the thermal behavior of an HTSC leads.

Previous models presented a limitation in considering the HTSC leads to be cooled by conduction only. In many applications, the HTSC leads are cooled by gas Nitrogen or gas Helium. For this, many authors have developed more rigorous analytical mathematical models that take into consideration convective cooling [8-10]. The

analytical model by Citver et al. [8], which is a transient one-dimensional energy balance model, takes into consideration variable conductivity, Joule Heating and convective heat transfer. The authors compare the model outputs with experimental data of a HTSC leads assembly made out of a combination of a HTS material and copper. The temperature of the copper component is modeled between room temperature and 80 K. The HTS portion of the lead is modeled from 80 K to 4.3 K. The authors found a discrepancy in the steady sate cooling flow and temperature between the experimentation and the model of 30 percent in the flow and 10 percent in the temperature, at a fixed point. Results showed that the burnout occurs on the warm end of the leads.

In more complex systems, as presented by Ünal and Chyu [9], a two-dimensional cylindrical model is employed. The authors investigated the behavior of a cylinder/wire type superconductor subjected to instantaneous thermal disturbances, characterized by a linear heat source. The model employed convective heat transfer and Joule heating and was simplified by considering constant thermophysical properties. Thermal modeling of HTSC has also been done by Koizumi et al. [10] for a cable-in-conduit conductor (CICC). The major application for the CICC was for fusion reactors. In this model, the governing equations were a one-dimensional fluid dynamics and heat conduction equations.

Also, many efforts have been made in modeling high temperature superconductors (HTS) thin-films. One of the most promising applications of HTS thin-film is a liquid nitrogen temperature bolometer. The bolometric mechanism is due to an increase in the film temperature caused by the irradiation, which results in a detectable change in the temperature-dependent electrical resistance of the film. Flik et al. [11] and

Phelan [12] apply a rigorous thermal radiation and heat conduction analysis to an HTS thin-film irradiated by an optical pulse and compared the predicted bolometric voltage response to experimental data. Variable thermophysical properties and contact resistance between the film and substrate were taken into account in a one-dimensional conduction equation and volumetric radiation heat source. This equation is used to calculate the temperature distribution. The radiation heat transfer is modeled based on the electromagnetic theory.

J.M. Koo and S. Park [13] employed a one dimensional radiation and conduction heat transfer to investigate the thermal response of HTSC thin-film detectors exposed to a pulse laser beam. Their model took into consideration the local radiation absorption based on the electromagnetic theory, thermal contact resistance at the interface between the film and substrate, and nonuniform initial condition for the temperature.

Malinowski [14] employed a numerical analysis of the evolution of normal zones in a composite superconductor based on the hyperbolic heat conduction equation. The model took into account the Joule heating and thermopysical properties of the material are assumed to be constant. Lewandowska and Malinowski [15] presented an analytical method for the calculating critical energies of uncooled composite superconductors based on the hyperbolic heat conduction equation. The mathematical model took into account: the finite speed of heat transport, temperature dependence of the Joule heat generation, finite duration and the finite length of thermal disturbances. The thermophysical parameters of the conductor are assumed constant. Results obtained were compared with those predicted by the parabolic heat conduction equation.

Lor and Chu [16] numerically analyzed the hyperbolic heat conduction problem in the film and substrate composites exposed to a heat flux on the exterior film surface. The model is a one-dimensional conduction and radiation, where radiation is modeled using the electromagnetic theory. Finally, Al-Odat et al. [17] investigated the superconductor thermal stability under the effect of the dual-phase-lag heat conduction model. It was found that the dual-phase-lag model predicted a wider stable region as compared with the parabolic and hyperbolic heat conduction models. The model took into account convective cooling, constant thermophysical properties and Joule heating.

As presented in this literature review, the majority of the work on thermal modeling of HTSC leads took in consideration convective cooling. To the best knowledge of the author, there is no work on modeling of HTSC leads under purely conduction and radiation cooling, employing variable thermophysical properties, including thermal conductivity and emissivity. The scenario presented in this investigation consisted of HTSC leads that operate between 17 K and 1.3 K. The material used is the superconductive material Magnesium Diboride (MgB_2), which has a superconductivity transition temperature of 39 K.

The recent discovery in 2001 of the 39 K superconductivity in MgB_2 by Nagamatsu et al. [18] brought interest from researchers, especially in the field of applied superconductivity. The superconductivity temperature of MgB_2 is far above the transition temperatures of other technical low temperature superconductors. For practical applications of superconductors, many efforts have been made to produce high current carrying conductors in wire and tape geometries [19, 20].

The MgB$_2$ is brittle and not easily deformable. Wires and tapes for technical applications have to be prepared as coated conductor or with techniques like the powder-in-tube (PIT) technique [19]. Different research groups have prepared PIT MgB$_2$ wires and tapes with different sheath materials like Ag, Cu, Fe, Nb, Ni, and Stainless Steel. For the HTC leads a PIT MgB$_2$ wire with Fe and Stainless Steel as sheath material will be used. Goldacker's research group in the Institut fur Physik, (Forschungszentrum Karlsruhe), in Germany prepared the wire employed in this investigation.

The herein developed model neglects the Joule heating, since for the temperature range of 17 K and 1.3 K the MgB$_2$ leads behave always as superconductors. These leads are cooled by a joint of cooper wire which is at 4 K and act as heat sink. This joint can be modeled as a constant 4 K heat sink. Optimization of the location of this heat sink is made to minimize the heat load at the cold end. The conductivity of the material is a strong function of temperature.

The objective of the investigation does not need prior knowledge of the transient behavior of the leads. The focus of this work is the steady state temperature distribution and heat dissipation at the low temperature of the HTSC lead. For this reason, the hyperbolic heat conduction equation is not employed. These conditions are satisfied by employing a one-dimensional conduction and radiation heat transfer model. Thus, the parabolic heat conduction is employed in this investigation. Due to the lack of emissivity data at low temperature for the material used in the assembly, and the complexity of the setup arrangement, a variable emissivity was selected to cover the entire range of no

19

radiation to a black body and thus be able to find the emissivity most suitable for our experimentation.

Table 2.1 summaries all the relevant work on thermal modeling of HTSC leads, presented in this literature review. It includes the type of thermal model and the most relevant parameters used in the model. On the other hand, previous experimental work has been done in HTSC current leads for space applications [1]. Tuttle et al. developed the original ASTRO-E HTSC leads. The thermal setup used by Tuttle et al. employed the use of three stages: a 17 K stage, a 4.2 K stage and a variable temperature stage from 4 K to 17 K. This setup does not represent entirely the environment of the HTSC leads assembly, because the lowest temperature that the HTSC leads will be exposed is 1.3 K. The experimental setup used in this investigation is presented in Chapter 3, which consists of three stages: 17 K stage, 4 K stage and 1.3 K stage.

Author	Type of Model	Relevant Parameters
S.Y. Seol, et al. (1997)	1-D Transient Heat Conduction	Joule Heating, Variable Thermal Conductivity
L. Malinowski (1999)	1-D Transient Heat Conduction	Joule Heating, Constant Thermal Conductivity
G. Citver, et al. (1999)	1-D Transient Conduction and Convective Heat Transfer	Joule Heating, Variable Thermal Conductivity
A. Ünal and M. Chyu (1995)	2-D Transient Conduction and Convective Heat Transfer	Cylindrical Coordinates, Joule Heating, Constant Thermal Conductivity
N. Koizumi, et al. (1996)	1-D Transient Conduction and Convective Heat Transfer	Fluid Flow Equation, Joule Heating, Variable Thermal Conductivity
P.E. Phelan (1995)	1-D Transient Conduction and Radiation Heat Transfer	Joule Heating, Constant Thermal Conductivity
M.I. Flik, et al. (1990)	1-D Transient Conduction and Radiation Heat Transfer	Variable Thermal Conductivity
J. Koo and S. Park (1998)	1-D Transient Conduction and Radiation Heat Transfer	Variable Thermal Conductivity
W. Lor and H. Chu (1999)	1-D Transient Hyperbolic Conduction and Radiation Heat Transfer	Constant Thermal Conductivity
M. Lewadowska and L. Malinowski (2001)	1-D Transient Hyperbolic Heat Conduction	Joule Heating, Constant Thermal Conductivity
L. Malinowski (1993)	1-D Transient Hyperbolic Heat Conduction	Joule Heating, Constant Thermal Conductivity
M. Al-Odat, et al. (2003)	1-D Transient Dual Phase-Lag Conduction Model	Joule Heating, Constant Thermal Conductivity
Present Work	1-D Steady Conduction and Radiation Heat Transfer	Variable Thermal Conductivity, Variable Emissivity

Table 2.1. Literature Review Summary Table

CHAPTER 3

XRS HTSC LEADS DEVELOPMENT

3.1 HTSC LEAD REQUIREMENTS

The HTSC lead assembly needs to satisfy some basic design requirements. The assembly must provide two leads able to conduct a current of 2.0 amps for the ADR magnet and ten leads capable of carrying 0.5 to 1.0 amps to operate two cryo-valves. The operation of these valves is for ground purposes only, employed in the filling of the Liquid Helium (LHe) cryostat before launch. The HTSC leads should have adequate critical currents at 17 K, which is the maximum operating temperature the leads will be exposed under normal operating conditions. On the other hand, the assembly must fit in the available space of 25 cm of length and a cross section of 0.75 cm by 2.5 cm.

As mentioned in Chapter 2, the HTSC leads must conduct as little heat as possible to the LHe cryostat. This is to increase the lifetime of the spacecraft. Additionally, it needs to operate in a nearly no-electrical resistance environment. The XRS cryostat has a vapor He vent line available, which under normal operating conditions operates at 4 K to intercept some of the heat conducted through the leads. In addition to the limiting space and the thermal requirements, the entire assembly should be capable of surviving the rocket's vibration and shock loads at launching, with low-frequency peak accelerations around 25g and an overall vibration environment of 8.5 grms [1].

3.2   EXPERIMENTAL EQUIPMENT

The equipment employed for the thermal experimentation of the prototype and the final XRS HTSC lead assembly is located at the Cryogenics and Fluids Branch laboratory facilities at NASA GSFC in Maryland. A brief description of the equipment and the experimental setup is presented in detail in the following sections.

3.2.1   EXPERIMENTAL DEWAR

A cryogenic Dewar is an insulated container that is specially designed to house an experimental assembly at very low temperatures.   It is designed to isolate the experimental assembly from the relatively hot environment of the laboratory. This type of equipment is needed in this investigation for the thermal experimentation in order to cool down the prototype from room temperature to a temperature range between 1.3 K and 17 K. To meet these requirements, a Janis Research, Inc. 19" Dewar was used, as shown in Figure 3.1.

This experimental Dewar consists mainly of three reservoirs. The first reservoir is the outer reservoir which holds a vacuum space.   The vacuum space covers the surroundings of other two reservoirs and the experimentation area. Before starting an experimental run the vacuum space should go down to a pressure of ~5.0 μTorr (6.67 x 10^{-4} Pa) to be able to transfer cryogens to the other two reservoirs. The second reservoir is used to store Liquid Nitrogen (LN) which provides a constant environment temperature of 77 K, and acts as an insulator for the inner reservoir. The third reservoir is the inner tank, which is thermally connected to a copper (Cu) base plate where the experiment

takes place. This reservoir uses LHe to provide a 4 K environment to the experimental setup, at atmospheric pressure. By reducing the pressure of this tank to ~1 Torr (133.3 Pa), the temperature of the LHe can go down to ~1.1 K.

Figure 3.1. Janis Research 19" Helium Dewar

The material employed in the construction of this Dewar is a heavy Aluminum alloy. It is thick enough to hold the thermal stresses and pressure differences. Since it is quite heavy, the use of a crane is needed to be able to reach the experimental section area inside the Dewar. Figure 3.2 shows several of the steps needed to reach the experimental setup area. The Dewar was turned around 180° using the crane, as shown in Figure 3.2a. Once it is rotated the Dewar bolts were removed to separate it into two sections. Then, the LN and LHe radiation shields or baffles were removed, as shown in Figures 3.2b and 3.2c, respectively. Finally, the experimental working area was reached and ready to be used, as shown in Figure 3.2d.

(a)

(b)

(c)
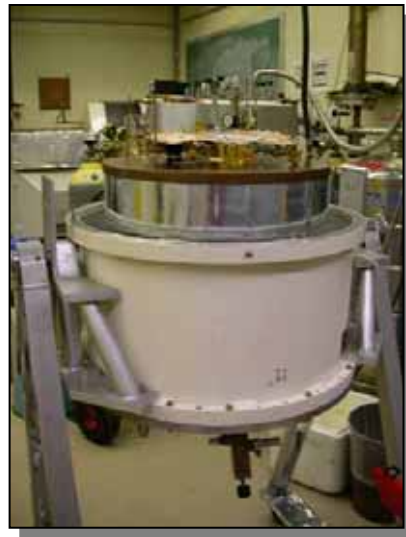
(d)

Figure 3.2. Janis Research 19" Dewar Disassembly

The experimental area consists mainly of a Cu base plate, as shown in Figure 3.3, which is thermally anchored with the LHe tank. The plate has an array of screw holes that are used to make the experimental setup. All the bolts used should be tight enough to

assure they will not get loose due to thermal stresses, where any loose part could create a non desired thermal short, causing failure of the entire experiment.
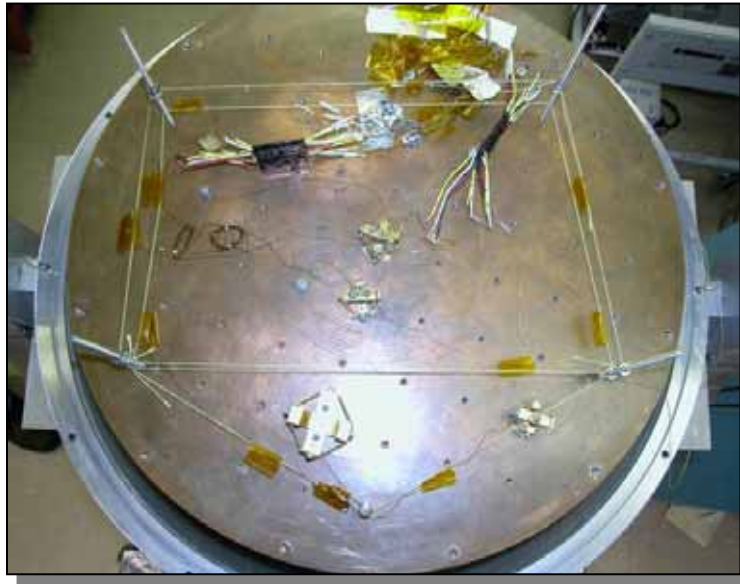
Figure 3.3. Experiment Copper Base Plate

3.3 PROTOTYPE DEVELOPMENT

An important part of any engineering design is the development of a prototype or prototype. In this investigation the prototype was made using a common cryogenic material, with all known cryogenic properties between 1.3 K and 17 K. One reason for using a material with known cryogenic properties was to be able to use the experimentation data to validate the computer thermal model. Another reason for using a different material was the unavailability of the MgB_2 superconductor during early stages of this research. Thus, the material used to develop the prototype was Stainless Steel Type 316 (SS316).

3.3.1 ASSEMBLY PROCEDURES

As part of the basic requirements, the HTSC leads prototype consisted of twelve SS316 wires with dimensions of 0.015" diameter and 12" length for each wire. Teflon or Polytetrafluoroethylene (PTFE) tubing was used in each of the SS316 wires for electrical insulation purposes. To meet the low heat conduction requirement for the cryostat, a joint of 0.016" diameter Cu wire and the SS316 was made in each of the wires using epoxy Stycast 2850FT, as shown in Figure 3.4a. Stycast 2850FT is one of the most common cryogenic epoxies and its data sheet is provided in Appendix A.

(a)   (b)
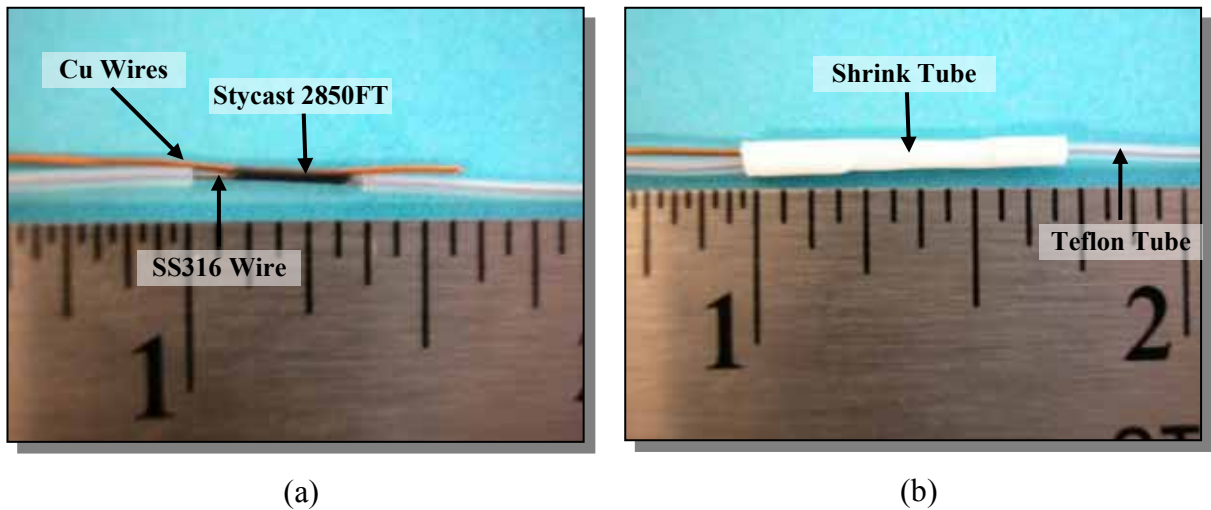
Figure 3.4. SS316-Copper Wire Stycast 2850FT Joint

The Cu wire, shown in Figure 3.4, becomes part of what is called the 4 K Heat Sink Link (HSL). This wire is electrically insulated to prevent an electrical short-circuit between wires. Since the end of the Cu wire was insulated, it was located over the PTFE tubing. After the Stycast 2850FT was dried, heat shrink tubing was used to cover the SS316-Cu wire joint, as shown in Figure 3.4b. The Stycast 2850FT was used to secure the joint, but its main purpose was to increase the contact area between the wires, to

increase the heat flow. The heat shrink tubing was used to provide support to the structure of the joint. The 4 K HSL will be ground to a 4 K stage to be able to keep the entire joint between the SS316 and Cu wires at 4 K.

Once this procedure was done to each of the twelve wires, all the wires were put together as one entire assembly. Then the Cu wires were twisted together to form the final 4 K heat sink link. To recreate flight conditions and to be able to use this prototype in an experimental setup, it was necessary to make a heat sink and source at each end of the wires, as shown in Figure 3.5. Stycast 2850FT was used to provide the thermal joint between the wires and the sink plates.
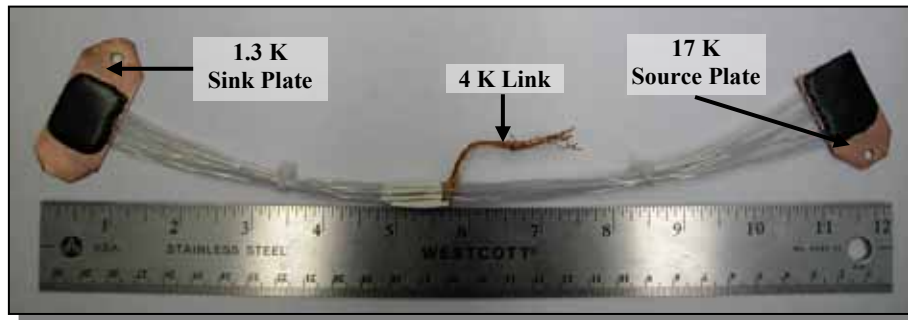
Figure 3.5. Experimental SS316 Prototype

3.3.2 PROTOTYPE EXPERIMENTAL SETUP

Once the prototype was completed and the Dewar experimental area was cleared, the experimental exercise was defined. This was needed to maximize the space and resources in the Dewar due to the fact that the Dewar has only twelve channels available for data acquisition. The objective of the prototype experimentation was to calculate the amount of heat that could be dissipated through a 4 K HSL from 17 K to 4 K. Three

thermal isolation stages were used in this setup, as shown in Figure 3.6. This provides a similar environment to the XRS, where each stage provided a constant temperature platform. Each stage or stand is made of gold plated copper and each has a Kevlar suspension for isolation from the Dewar Cu base plate.
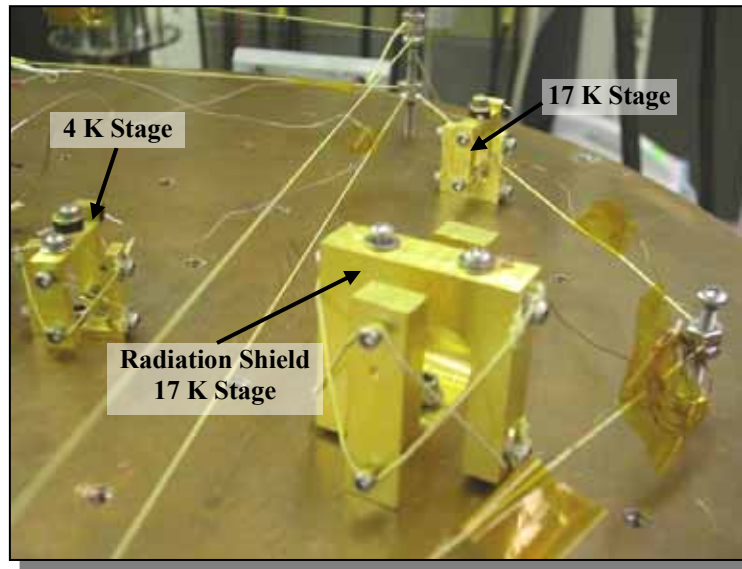
Figure 3.6. Thermal Isolation Stands Experiment Setup

The first stage provides a constant 17 K platform and it was used at one end of the prototype wires. The second stage was used to provide the 4 K platform and it was used for the prototype heat sink. The last stage was employed to support and provide a 17 K radiation shield stage made of a sheet of Cu and, after assembly, the prototype was covered. The remaining end of the prototype, which is the cold end section, was attached directly to the Dewar Cu base plate. To reach the desired temperature in each of the stages, a heater was used to increase the temperature of the stage and a thermometer to read the temperature.

Four screw poles with Kevlar strings around them were used for routing the heater and thermometer wires and, for supporting the radiation shield. The low thermal conductivity of the Kevlar was used to provide isolation to the wires. All the heater wires were routed on one side and, the thermometer wires to the other side of the Dewar. It is extremely important that the heater wires do not touch at any time the thermometer wires to prevent inaccuracy in the readings. Kapton tape was used to keep the wires together with the Kevlar string. To have a better understanding of these stages, Figures 3.7 and 3.8 show the 17 K and 4 K stages and its components.
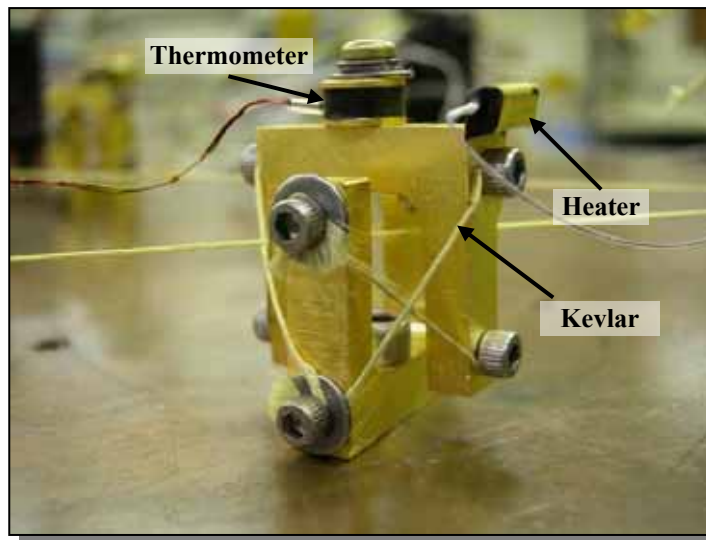
Figure 3.7. 17 K Stage Stand

Each of the stages has a Kevlar suspension. This is used to isolate the upper part from the lower part of the stage, which is thermally connected with the Cu plate. The prototype is connected to the upper part of the stage. The 4 K heat sink stage consists of a thermometer, a heater and a heat sink link to the Dewar Cu base plate, which during experimentation is maintained at 1.3 K, as shown in Figure 3.8. This link provided faster

cooling for this stage. The 17 K stand and the radiation shield consisted of a thermometer and a heater.

The thermometers used in each of the stages in the experimental setup were the Lakeshore Cernox model, which are electrical resistance sensor with low magnetic field-induced errors. It has high sensitivity at low temperatures and good sensitivity over a broad range (0.3 K to 420 K). Further information on the Lakeshore Cernox Thermometer is included in Appendix A.
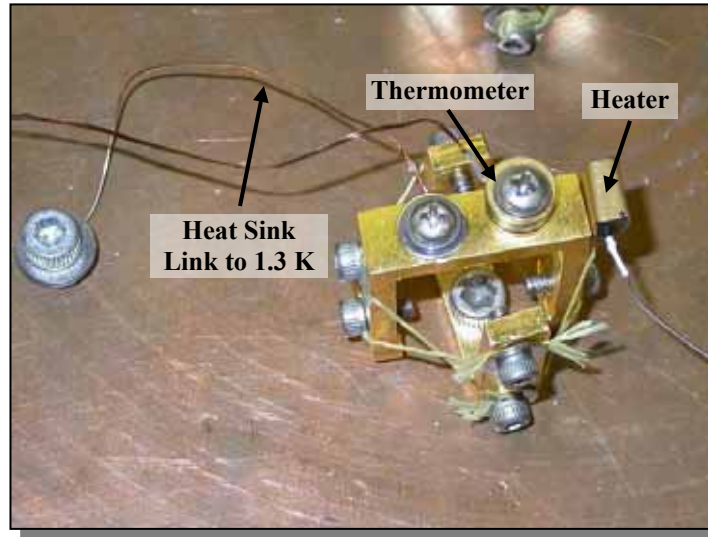
Figure 3.8. 4 K Heat Sink Stand

3.3.3   COOL-DOWN PROCESS

Once the experiment setup was ready and the Dewar was closed, assuring that there were no thermal shorts in any place, the experimental setup was cooled down. At this phase of the experimentation, the prototype was not yet on the system. The first step is to calibrate the stages and then, employed the prototype. In order to make the calibration or run the experiment, it is necessary to cool down the Dewar from ~293K

(room temperature) to 1.3 K. All the air inside the Dewar is taking out by using a vacuum pump to reach a desired pressure of ~5.0 μTorr (6.67 x 10^{-4} Pa). During normal conditions it takes ~24 hours to attain this conditions. Once the vacuum pressure is reached the LN and LHe reservoir are filled with LN.

Why LN first instead of LHe which is at lower temperature? It is known that the enthalpy of common materials used for constructing cryostat (stainless steel, copper, aluminium, etc) drops rapidly when decrease temperature. This, coupled with the low cost of LN and its high heat of vaporization (relative to helium), makes it the natural choice to cool the Dewar first from room temperature to 77 K, Figure 3.9.
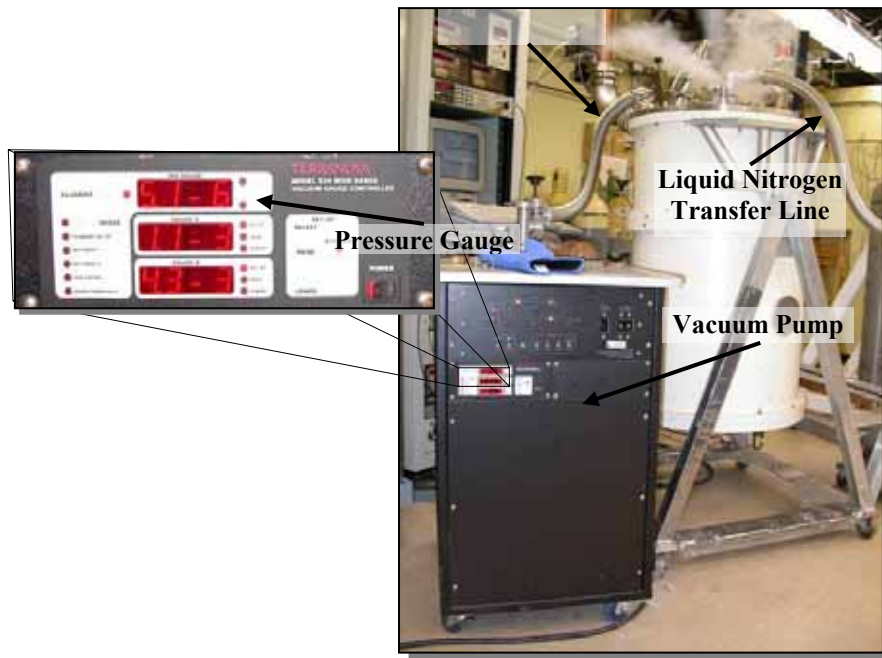
Figure 3.9. Cooling Down Setup

The heat of evaporation for helium at atmospheric pressure, when changing from liquid to the gas, is about 2.6 kJ/L at its normal boiling temperature of 4.2 K. This is a

rather small number compared to the enthalpy of helium gas between 4.2 K and room temperature, which is about 200 kJ/L and 64 kJ/L between 4.2 K and 77 K. Liquid Nitrogen is used to pre-cooling to 77 K, because its latent heat is 69 times the evaporation heat of LHe and is about and order of magnitude cheaper [21].

In summary, the entire process from the vacuum cycle to start running the experiment takes approximately 3 days. The entire cooling down process from room temperature to 1.3 K takes approximately 38 hours, Figure 3.10. Therefore, if the time needed before transferring LN is approximately 24 hour, it means that to start an experiment, it takes approximately 2.5 days to reach the desired temperature.

Cooling-Down Process
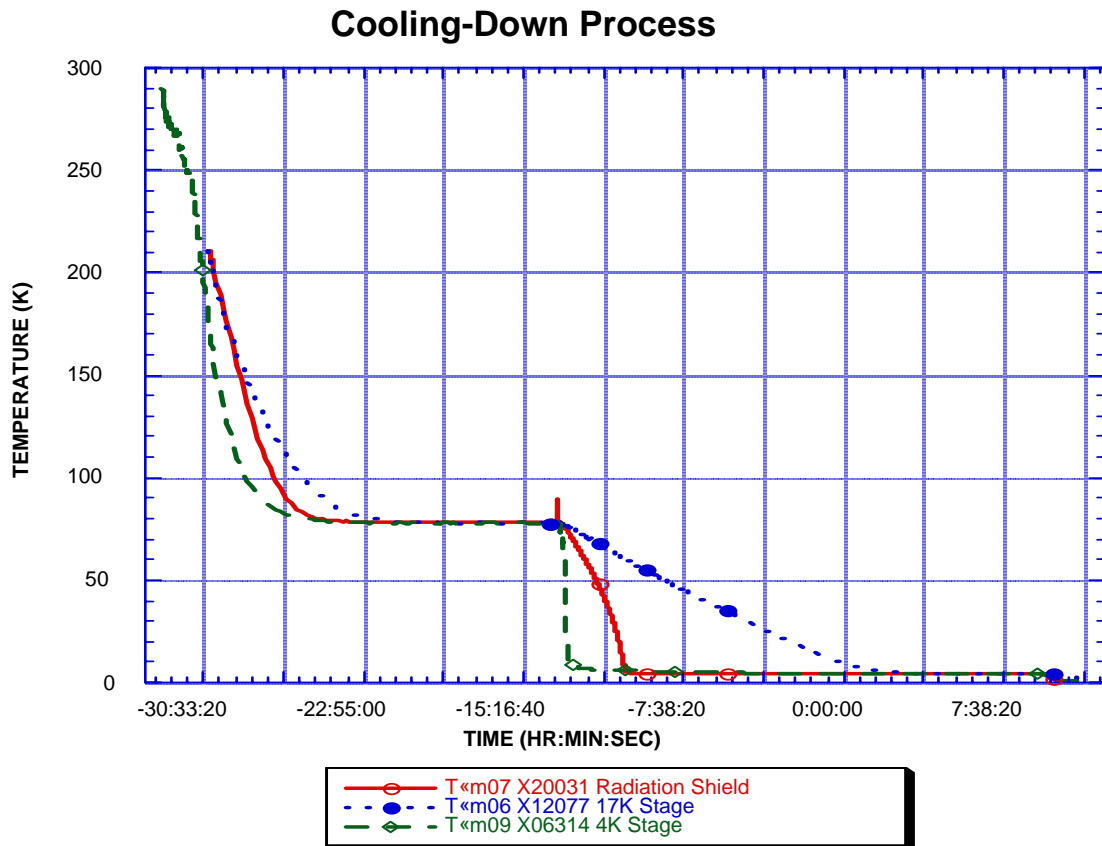
Figure 3.10. Experimental Cooling Down Process

33

3.3.4 STAGES CALIBRATION

Once the 1.3 K steady temperature was reached on the entire system, the testing setup was calibrated at each of the stages. At this phase of the experimentation, the prototype was not yet on the system. The main objective of the calibration of the stages was to calculate the heating power needed for heating to keep a steady temperature on the stages. This measurement served as a baseline for calculating the heat load through the leads. The first step in this process was a 4-wire resistance measurement to calculate the resistance of each of the components. Once this information was entered in the data acquisition software, the experimental calibration could start, and different power values were applied. The data acquisition system consisted of a Macintosh computer using MACACQUISITION software, a pressure controller and three current sources for each stage, as shown in Figure 3.11.
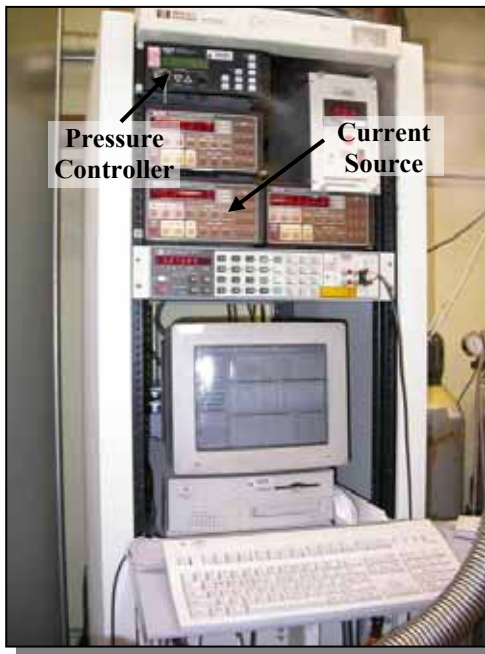
Figure 3.11. Data Acquisition System and Current Sources

Steady state was reached on each of the stages at the same time before making the final measurement of temperature and power. In the first calibration run, the 4 K Stage Cu link to 1.3 K Dewar Cu base plate was too strong, needing ~13,800 µW (~3 mA) to keep a 4 K temperature in the stage. It is expected that ~600µW will be transferred through the HSL and, therefore, a good calibration should be around twice this load. By decreasing the area and increasing the length of the link as given by the Fourier Law, the new link for the 4 K Stage was reduced to 1,281 µW to keep it 4 K temperature. On the other hand, the 17 K stage needed 78 µW and the Radiation Shield ~67,000 µW to keep a 17 K constant temperature.

3.3.5 PROTOTYPE THERMAL TEST

After calibrating and calculating the power needed for each stage to keep a steady temperature, the prototype was mounted in the testing Dewar, as shown in Figure 3.12. The prototype warm end was mounted at the 17 K stage, the 4 K heat sink link to the 4 K stage and, the cold end to the copper base plate at 1.3 K. Once the prototype was in place, a calibration run was made on the entire setup to calculate the power needed in each stage to keep their respective temperatures. The difference in power between the runs in each stage was the amount of heat input and output through the leads.

Figure 3.13 shows a close-up of the prototype warm end connected to the 17 K stage. The heat source copper plate was mounted between the thermometer and the stage stand in order to have a closer reading of the temperature source. It was expected to obtain a small source of error in the temperature reading. This was due to the location of

the thermometer in the copper plate and the prototype.   It was expected that the temperature difference between the two ends of the heat source copper plate to be ~1 mK.
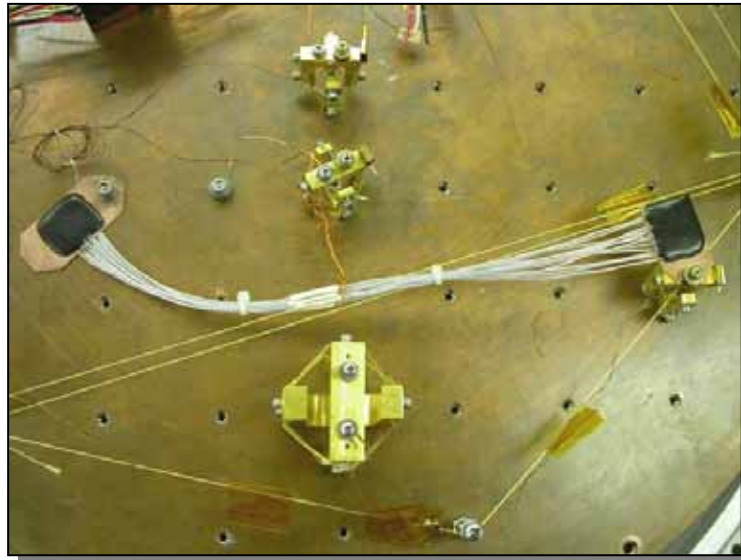
Figure 3.12. Prototype Setup
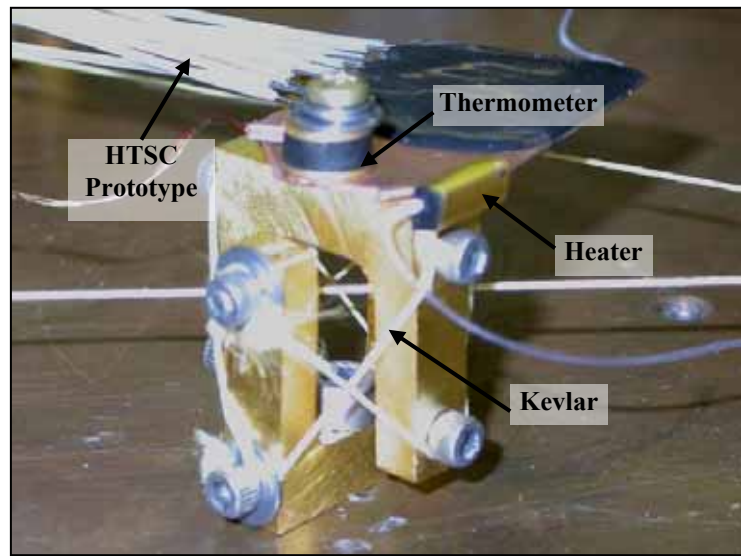
Figure 3.13. 17 K Thermal Isolation Stand

The 4 K heat sink link was connected using two wires in the top bolt and two in the bottom bolt of the Kevlar suspension string, as shown in Figure 3.14. With this arrangement the heat input to the stage could come from the link and the heater which are at opposite sides. This way, the thermometer, which is in a mid point between the two heat sources, could have a better reading of the real temperature of the stage.
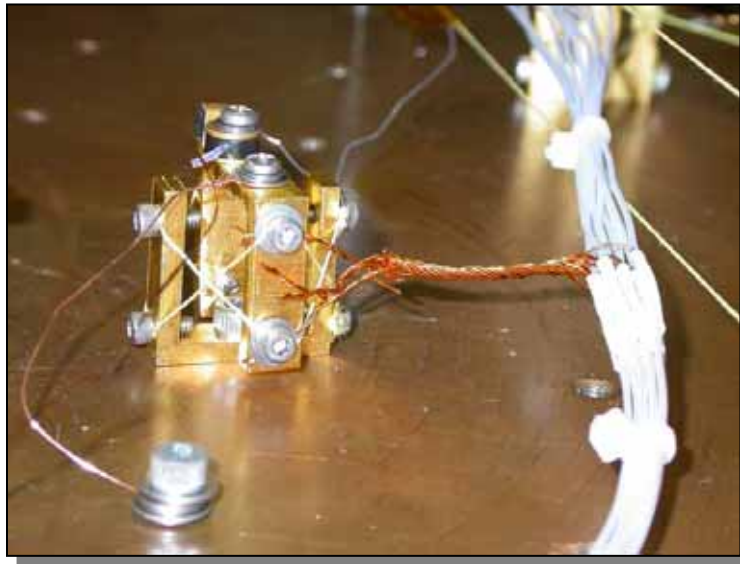
Figure 3.14. 4 K Heat Sink Prototype Link Assembly

The last part in the experimental setup was the integration of the radiation shield, which is supported by the isolation stand and several Kevlar strings, Figure 3.15. Once the setup was ready, the Dewar was closed and the cooling procedure was applied again to reach the desired temperature range. Thermal calibration for the entire setup was performed successfully. The 4 K stage needed 1,142 µW to keep a 4 K temperature. The 17 K stage needed 204 µW and the Radiation Shield ~67,000 µW to be kept at a constant temperature of 17 K. Therefore, the difference of each stage from calibration was 139 µW for the 4 K stage and 126 µW for the 17 K stage.
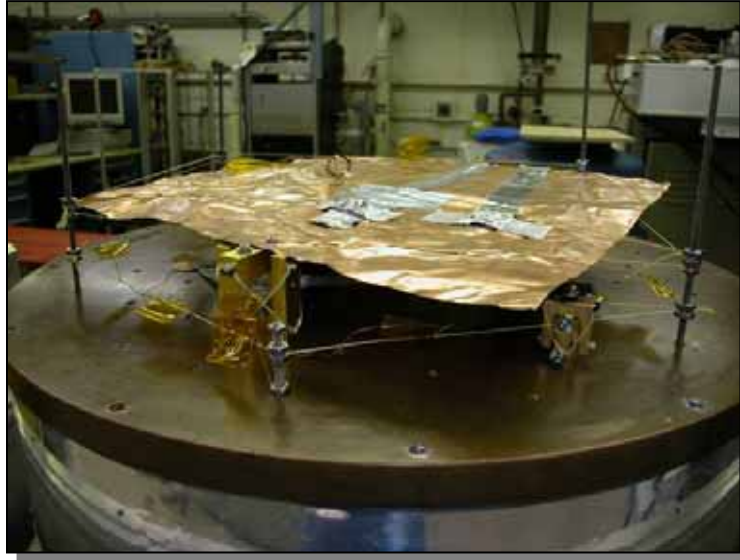
Figure 3.15. 17 K Radiation Shield

3.4 MAGNESIUM DIBORIDE (MgB$_2$) DESIGN

The final design of the HTSC leads assembly was made of MgB$_2$. Through the development of the prototype, new modifications were made as needed for the final design, especially in the 4 K HSL. On the other hand, the prototype considered mostly the thermal aspect of the design and it was not focused entirely on the structural aspect to support the rocket vibration.

3.4.1 ASSEMBLY PROCEDURES

One of the main concerns on the new HTSC design was how to keep the wires attached to the Kevlar suspension strings while supporting the rocket vibration. It looked like using just a few zip-ties straps could secure the wires in the radial direction to the Kevlar, but the assembly still needed to be also fixed axially. The new HTSC design should provide radial and axial support for vibration purposes and heat sinking to 4 K.

On the other hand, the 4 K HSL of the prototype showed to be thermally suitable, but poorly designed for vibrations. The heavy mass in the center of the prototype could make permanent damages to the lead assembly during launch. Therefore, the mass of the copper wire heat sink link had to be reduced for vibration purposes. To solve the vibration issue without sacrificing thermal performance, the new heat sink joint consisted of a 1/2" long G-10 piece with 12 grooves around it and, a single hole in the center for the Kevlar support string, as shown in Figure 3.16.

Figure 3.16. G-10 Heat Sink

The new design provided each of the SS316 wires to be bonded with Stycast 2850FT to the G-10 piece. A single 0.02" diameter copper wire is used to provide the 4 K heat sink. This eliminates the use of 12 single copper wires in each SS316 wire and potentially reduces weight. To provide axial support to the HTS wires, the G-10 piece was bonded together with the Kevlar string exactly the same way the first HTS was built, which satisfies the previously mentioned requirements in a 25g vibration test.

The final configuration of the Kevlar suspension with the G-10 heat sink and centering rings epoxied together is shown in Figure 3.20. The next step was to epoxy the copper wire in the radial direction to the heat sink and install pins connectors to the end of each wire in order to run a thermal test.
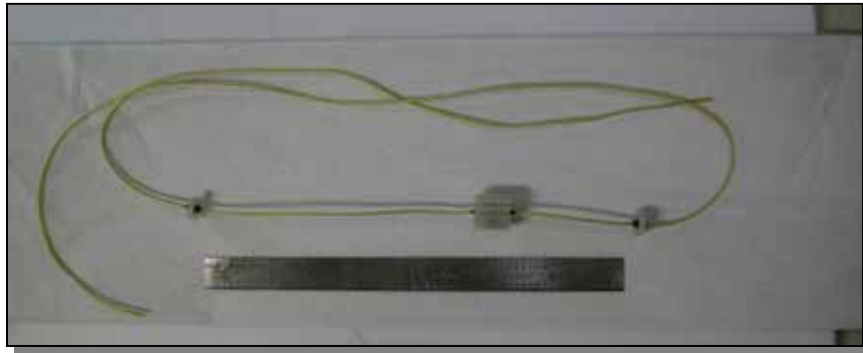
Figure 3.17. G-10 Heat Sink and Centering Rings in Kevlar Suspension

Once the Kevlar suspension had the G-10 pieces bonded with Stycast 2850FT, all twelve MgB_2 wires were placed in each grove of the G-10 heat sink. A 1" heat shrink tube was used to prevent the wire for breaking near the G-10 heat sink because bending of the wire during assembly. This is important, since the MgB_2 wire was manufactured using the PIT technique. This means that the superconductor could be easily broken by bending during the construction process. Figure 3.18 shows the G-10 heat sink with all the MgB_2 wires on the groves.

Once all the MgB_2 wires were located in the groves, they were put in place the 4 K HSL. This last one was made using a 0.024" diameter copper wire that was bent in a helix form to cover the G-10 heat sink and all the MgB_2 wires.

This wire has a relative high thermal conductivity to be able to conduct the maximum heat coming from the HTSC leads.
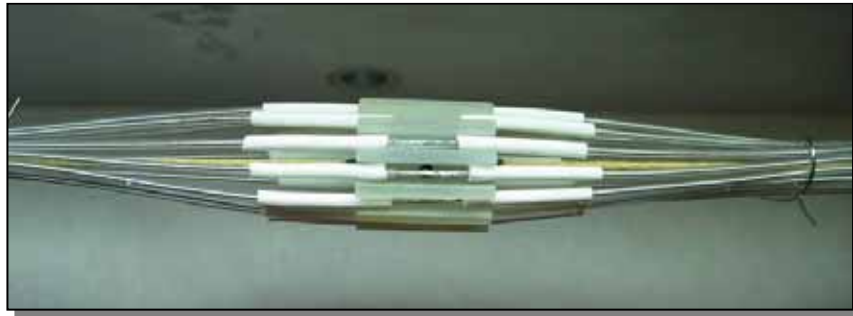
Figure 3.18. G-10 Heat Sink with Wires in Place

Figure 3.19 shows the 4 K HSL before assembly. The 4 K HSL used a piece of heat shrink tube that is used to provide more strength and structure to the wire to prevent breaking due to bending during assembly.
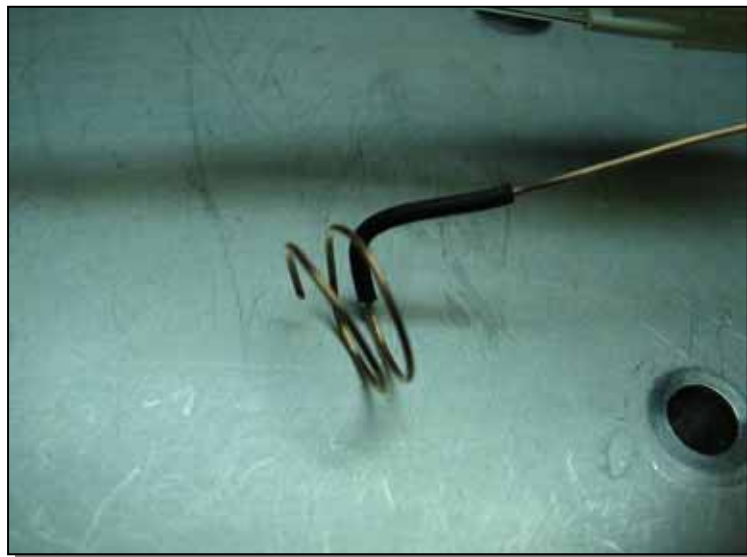
Figure 3.19. 4 K Copper Heat Sink Wire

Once the wire was in place over the G-10 heat sink and MgB$_2$ wires, as shown in Figure 3.20, the HSL, the MgB$_2$ wires and the G-10 heat sink were bonded with Stycast 2850FT. In this case the Stycast 2850FT would provide strength to the joint and support for radial and axial vibrations. The Stycast 2850FT also increased the thermal contact area between the MgB$_2$ wires and the 4 K HSL to provide a good heat conduction without making an electrical short between the wires. Figure 3.21 shows the final 4 K heat sink after the Stycast 2850FT dried.
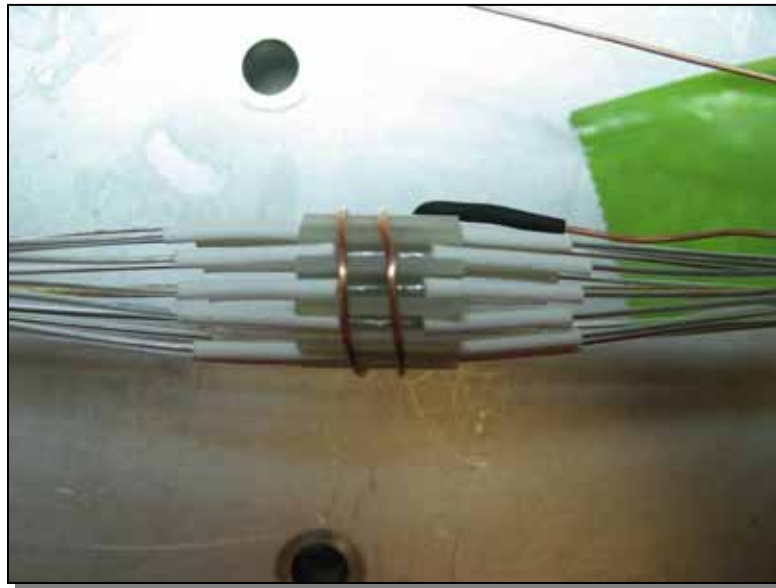
Figure 3.20. 4 K Copper Heat Sink Wire in Place

In summary, the final HTSC lead assembly has new features compared with the old XRS HTSC lead assembly. It provides a better safety margin to the NbTi wires keeping them below 4 K and preventing them from reach the transition temperature of 9 K and burnout.
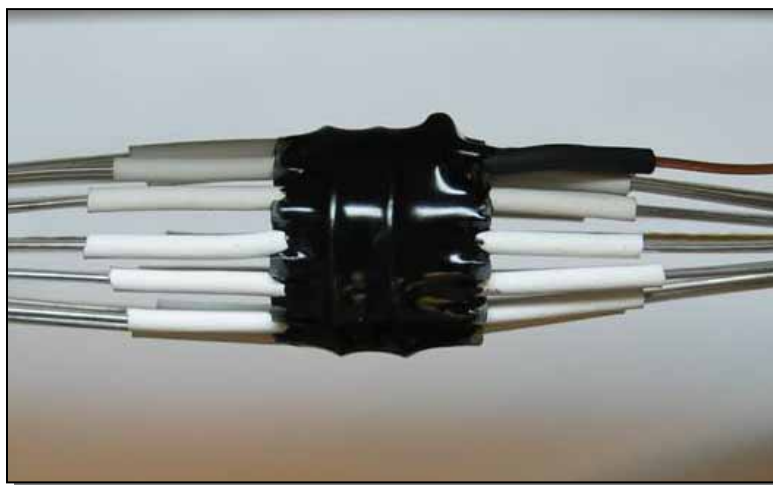
Figure 3.21. 4 K Copper Heat Sink Wire Bonded Tangential to the G-10

The new design also eliminates the use of a fiberglass tube along the leads and the use of the YBCO filaments which are very fragile to work with. Figure 3.22 shows a diagram of the comparison between the old and new HTSC lead design.
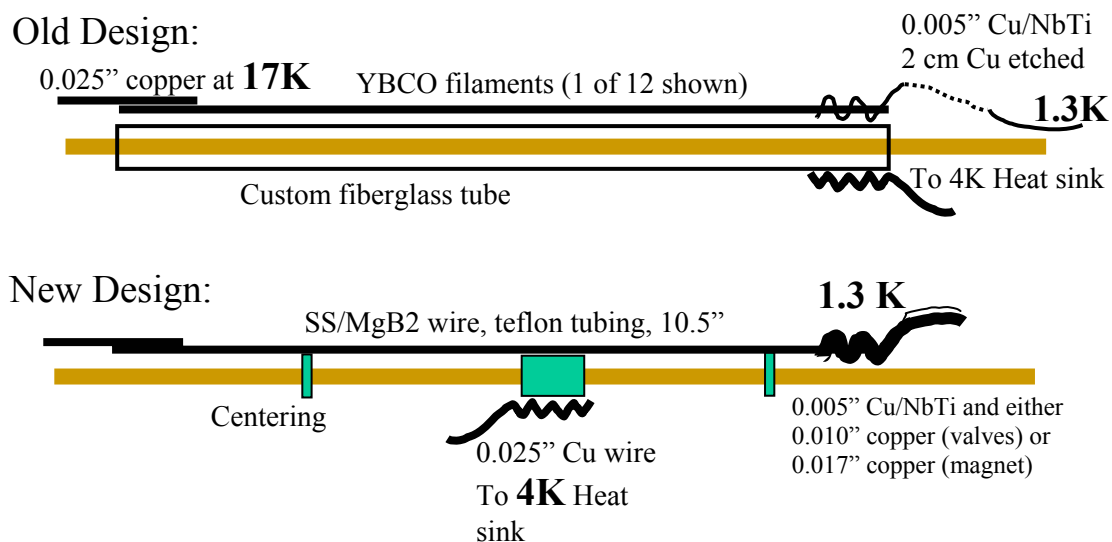
Figure 3.22. Comparison between the Old and New Design

The last procedure, before the HSTC lead assembly could be used in the final configuration, was welding the copper wires at the warm side (connected to the cooper wires coming from the current source) and welding the NbTi wires that goes down to the ADR magnet at the cold side. Figure 3.23 show the final MgB$_2$ HTSC lead assembly.
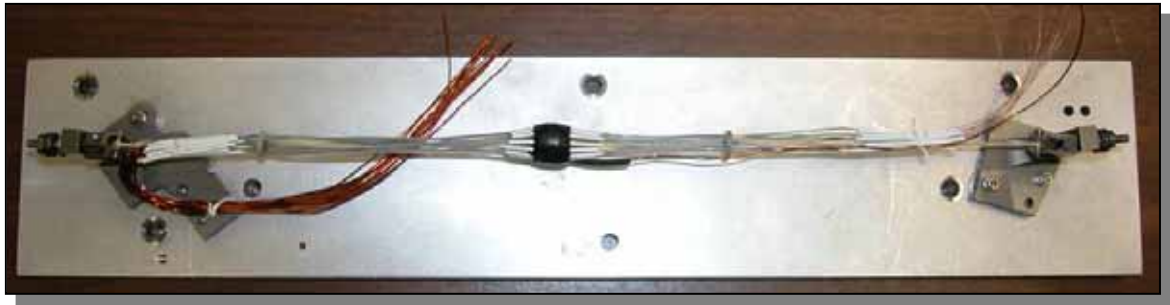
Figure 3.23. Final Suspended HTSC Lead Assembly

3.4.2 EXPERIMENTAL SETUP

The experimental setup for the MgB$_2$ HTSC lead assembly was different from the prototype. In principle the experimental objective was the same as the prototype setup, which was to measure the heat load through the assembly. The main difference in this setup was the completeness of the assembly in its final configuration. The assembly was mounted in the Kevlar suspension with the copper and NbTi wires welded to it. This setup, as shown in Figure 3.24, consisted of different stages with their respective thermometers and heaters, to keep a constant temperature. The first stage was the 17 K stage which is connected with the cooper wires. This stage was made of a cooper sheet and was suspended in a Kevlar string. The purpose of isolating this stage was to ensure that the power input to the heater was the same heat power going through the HTSC lead.

Successively, the 4 K stage, is pretty similar to the one used for the prototype, having the same configuration of thermometer, heater and heat sink link to the base plate. The next stage was a new stage not used in the prototype setup. A large Aluminum plate at 17 K was used to simulate the same environment and configuration of the suspension in the spacecraft.
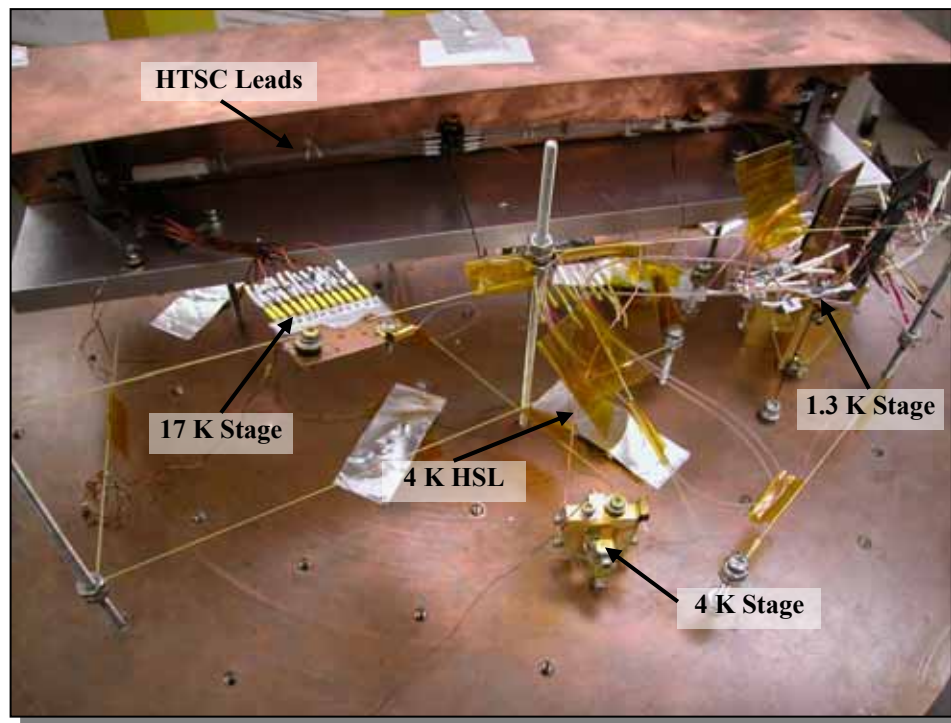
Figure 3.24. Final HTSC Lead Assembly Setup

This stage included a radiation shield of a copper plate, thus the assembly could be exposed to the worst case scenario, having a 17 K radiation around it from three sides. The last stage was the 1.3 K stage which is used to connect the NbTi wires, as shown in Figure 3.25.

Different from the prototype experimentation, this setup could be used for two experiments. The first one consisted on the calculation of heat load through the assembly. The second experiment was to pass electric current while holding each stage temperature. This last experimentation is made to qualify the assembly for flight use.
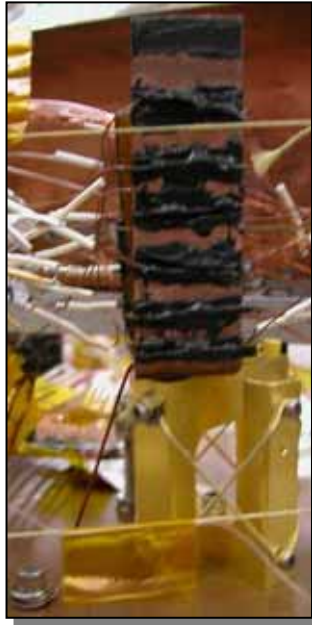
Figure 3.25. 1.3 K Setup Stage

Another new feature of this experimental setup is the use of thermometers in two locations. The first location was at the 4 K heat sink and it was used to measure the temperature gradient in the HSL between the 4 K heat sink and the 4 K stage. The thermometer was put in place using varnish, Figure 3.26.

Figure 3.26. 4 K Heat Sink Thermometer Stage

3.4.3   MgB₂ THERMAL TEST

After each stage was calibrated, the final HTSC lead assembly was successfully tested; thermally and electrically. Thermal loads measurements were made on vacuum through the assembly.

3.5 LESSONS LEARNED

During the construction phase of the prototype, a first attempt was made to locate the heat sink and heat source at the ends of the wires. This required welding all the SS316 wires to a Cu plate. This welding process implies to tin the Cu plates and each of the wires before welding them, which was a very tedious process. During the welding process two of the SS316-Cu wire joint broke in the epoxy region. This event led to a new design for the SS316-Copper wire joint to prevent this from happening again. The two broken joints were replaced with two new wires for the final prototype. On the other hand, Stycast 2850FT was used for the heat sink plates due to the complexity of welding SS316 at the end of the wires.

The 4 K HSL connection was quite challenging, due to the limiting space in the stage. In the HSL there were twelve copper wires available to be connected into the stage, but it was not feasible to connect all the wires since there was not enough space. As a first attempt to resolve this issue, some wires were connected to the same bolt of the 1.3 K HSL. The problem in doing so was that the stand was already calibrated. By removing the bolt on the stage and connecting it to the HSL wires, the pressure in the bolt after connecting the wires would be different to the one initially calibrated. This could result in another cool down and new a calibration run. Therefore, if the bolt is removed, this could cause another source of error, due to thermal conduction between two connecting surface, which depends on the pressure between the two and, therefore, this option was discarded.

CHAPTER 4

THERMAL MODEL

In general, heat may be transferred by conduction, convection, and radiation. In most low-temperature applications, heat transfer by convection is not significant because of the partial evacuation of gases from the interior of the cryostat. Basically, heat transfer takes place in low-temperature systems by conduction, through the residual low-pressure gas; conduction through the solids that interconnect the various parts of the cryostat, and by radiation. In addition, Joule heating in electrical leads, eddy current heating, mechanical vibration, and absorption of gases may also contribute to the total heat transfer in the system.

For heat conduction, the heat flux equation is know as the Fourier Law. For one-dimensional linear conduction the heat flux q'' through a solid of cross-section A and thermal conductivity k under a temperature gradient dT/dx is given by,

$$q_x'' = -k(T)\frac{dT}{dx} \qquad (4.1)$$

In most cases if the ends of a solid bar, of uniform cross-section and length L are at T_1 and T_2, with a linear temperature distribution for steady state and constant k, as shown in Figure 4.1, equation 4.1 can be written as,

$$q_x = -kA_c\frac{T_2 - T_1}{dx} \qquad (4.2)$$

where A_c is the cylinder's cross sectional area.
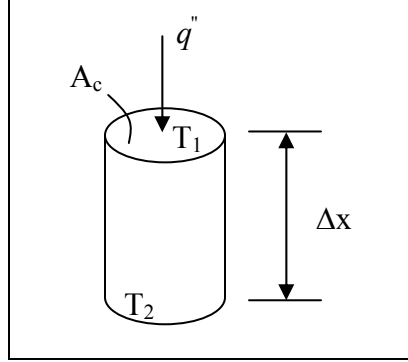
Figure 4.1. Heat Conduction in a Bar

In most cryogenics systems, the thermal conductivity k depends on the temperature. Thus, a relationship between thermal conductivity and temperature was obtained. To understand how thermal conductivity depends upon temperature, especially at low temperatures, it is useful to understand the basic mechanisms for energy transport through materials. In general, it is known that nearly all physical properties of a solid depend upon lattice vibration, also known as phonon conduction, or motion of the atoms in the solid. Since the thermal energy of a solid can be treated in terms of phonons, the solid becomes comparable to a container filled with a phonon gas. With this model the thermal conductivity of a solid can be calculated in terms of the thermal conductivity of a gas. Therefore, based on the classical kinetic theory of gases, the thermal conductivity can be expressed as,

$$k = \frac{1}{3} C_v \bar{v} \lambda \qquad\qquad \textbf{(4.3)}$$

where C_v is the specific heat of the phonons (the lattice specific heat), $\bar{v}$ the velocity of propagation of the phonons which travel at the speed of sound, and λ the mean free path of the phonons between collisions.

To find the thermal conductivity, the specific heat at low temperatures must be known. Although the specific heat is not used in the thermal model, due to steady state condition, a literature review is presented in the following pages for obtaining an expression for the specific heat and substitute it in Equation 4.3. A thermal conductivity expression could be found from Equation 4.3, since at very low temperatures the velocity of propagation of the phonons and the mean free path remains constant. Thus, the thermal conductivity is proportional to the expression found for the specific heat.

In early 1900's, a number of theories based on quantum theory were developed to predict a variation of the lattice specific heat with temperature in solids. Two of the best-known theories were developed by Einstein and Debye [21, 31, 32]. The theory of lattice specific heat was basically solved by Einstein, who introduced the idea of quantized oscillation of the atoms. Einstein established a relation for the specific heat at constant volume of the form,

$$C_{vl} = 3\Re\left(\frac{\theta_E}{T}\right)^2 \frac{e^{\theta_E/T}}{\left(e^{\theta_E/T} - 1\right)^2} \tag{4.4}$$

where $\Re$ is the universal gas constant and θ_E is the characteristic Einstein temperature, which is defined as hv_E/K and has temperature units; were h is Planck's constant, v_E

the single frequency of vibration, and K is Boltzmann constant [21, 31, 32]. The expression fits experimental data quite well for all materials except for low temperatures, where it drops below the experimental values. At intermediate and high temperatures it provides good curve fitting, and provides a limiting value of $3\Re$ at high temperature.

In later years Debye [21, 31, 32] made a major advances in the theory of heat capacity at low temperatures by treating a solid as an infinite elastic continuum and considering the excitement of all possible standing waves in the material. The Debye model gives the following expression for the lattice heat capacity per mole:

$$C_{vl} = 9\Re\left(\frac{T}{\theta_D}\right)^3 \int_0^{\theta_D/T} \frac{x^4 e^x}{\left(e^x - 1\right)^2}\, dx = 3\Re\left(\frac{T}{\theta_D}\right)^3 D\left(\frac{T}{\theta_D}\right) \qquad (4.5)$$

where $\Re$ is the universal gas constant per mole, T is the absolute temperature, θ_D the characteristic Debye temperature defined as $h v / K$ and x is a dimensionless variable defined as $h v_m / KT$. Here h is Planck's constant, v_m maximum frequency of vibration and K the Boltzmann constant. The Debye temperature is the temperature of a crystal's highest normal mode of vibration, i.e., the highest temperature that can be achieved due to a single normal vibration. At low temperatures ($T < \theta_D/12$), the Debye function approaches a constant value of $4\pi^4/5$; thus, the specific heat at temperatures less than $\theta_D/12$ may be expressed as,

$$C_{vl} = \left(\frac{12\pi^4 \Re}{5}\right)\left(\frac{T}{\theta_D}\right)^3 = 464.5\left(\frac{T}{\theta_D}\right)^3 = AT^3 \qquad (4.6)$$

where A is a constant (cal/g mol K).

The temperature dependence of the thermal conductivity is given by the temperature dependence of the specific heat as shown in Equation 4.3. A relationship between the specific heat and conductivity can be expressed as,

$$k \propto C_v \propto T^3 \tag{4.7}$$

Therefore, the conductivity can be expressed as a cubic function of temperature as,

$$k = k_0 + k_1 T + k_2 T^2 + k_3 T^3 \tag{4.8}$$

This equation is not valid for absolute zero. The range of temperature where this function is valid depends of the material were the constant values are obtained experimentally. To be able to find the heat conduction equation with the conductivity as function of temperature, Equation 4.8 is integrated between a low temperature T_L to a high temperature T_H. It was found that the thermal conductivity integral K_T to be:

$$K_T = k_0(T_H - T_L) + \frac{k_1}{2}\left(T_H^2 - T_L^2\right) + \frac{k_2}{3}\left(T_H^3 - T_L^3\right) + \frac{k_3}{4}\left(T_H^4 - T_L^4\right) \tag{4.9}$$

and, therefore, the heat flow rate can be defined as,

$$Q_C = \left[k_0(T_H - T_L) + \frac{k_1}{2}\left(T_H^2 - T_L^2\right) + \frac{k_2}{3}\left(T_H^3 - T_L^3\right) + \frac{k_3}{4}\left(T_H^4 - T_L^4\right) \right] \frac{A}{\Delta x} \tag{4.10}$$

Table 4.1 shows the constant values for SS316 and PTFE and Figure 2.1 shows the plot of theses values.

Material	Range (K)	K₀	K₁	k₂	k₃
SS316	4 → 40	2.77792E-05	6.50691E-04	3.10766E-05	-4.34032E-07
PTFE	5 → 80	1.6119E-04	8.9238E-05	-1.4482E-06	8.3371E-09

Table 4.1. Material Constants for the Conductivity Function
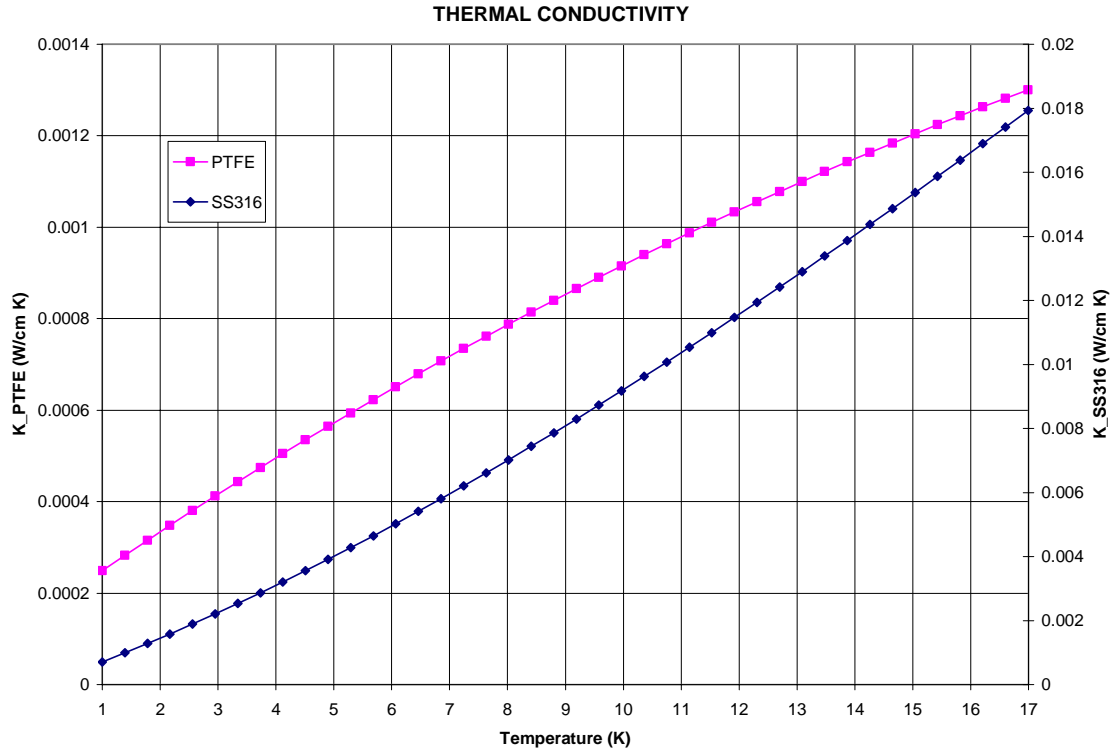
Figure 4.2. Thermal Conductivity of the SS316 and PTFE between 1.3 K and 17 K.

As shown in Figure 4.2, the thermal conductivity decreases strongly with decreasing temperature. The range of temperature where these functions were calibrated does not cover the entire 1.3 K to 17 K range, as shown on Table 4.1. Therefore, this represents a source of error for the model calculations.

Another source of heat transfer is by radiation. A perfect black body may be defined as one which absorbs all radiation falling upon it. For a black body at a temperature *T*, the total radiant energy emitted per second unit area is given by the Stefan-Boltzman Law.

$$q_x^{"} = \sigma A T^4 \tag{4.11}$$

For non-metallic surfaces such as glass, polymers and baked varnishes, in cryogenic equipment, emissivities are in the neighborhood of 0.9.

Now that the equations that describe the heat conduction and radiation are known, the next step in the model development is to apply these equations to the HTSC leads problem. The model considers one dimensional heat transfer. Two radiation bodies at 17 K and 1.3 K, respectively, are used to simulate the experimental environment. To simplify the model, a single is simulated, where the entire prototype simulation is twelve times the model outputs. The wire was divided into two sections: a warm side, which is between 17 K and 4 K and, a cold side between 4 K and 1.3 K. This division was done since there are three areas for which the temperature is known. These areas are the warm end which is at 17 K; the cold end, which is at 1.3 K; and the interface between them which is at 4 K. A single wire schematic is shown in Figure 4.3.
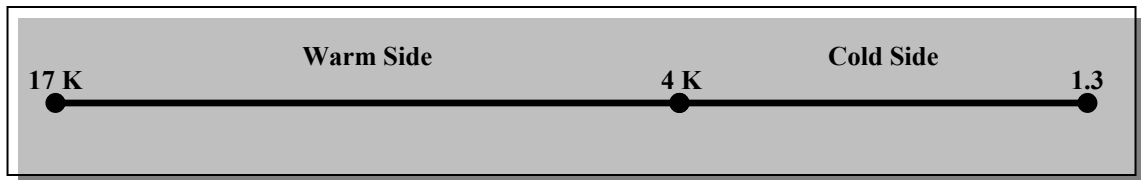
Figure 4.3. Know Temperatures in the Prototype Wire Model

The cold-warm interface is the simplest model for the 4 K heat sink stage, because it is modeled by a single node at a constant temperature. Each side is divided in nodes as shown in Figure 4.4 which also shows a schematic of the entire problem assembly.
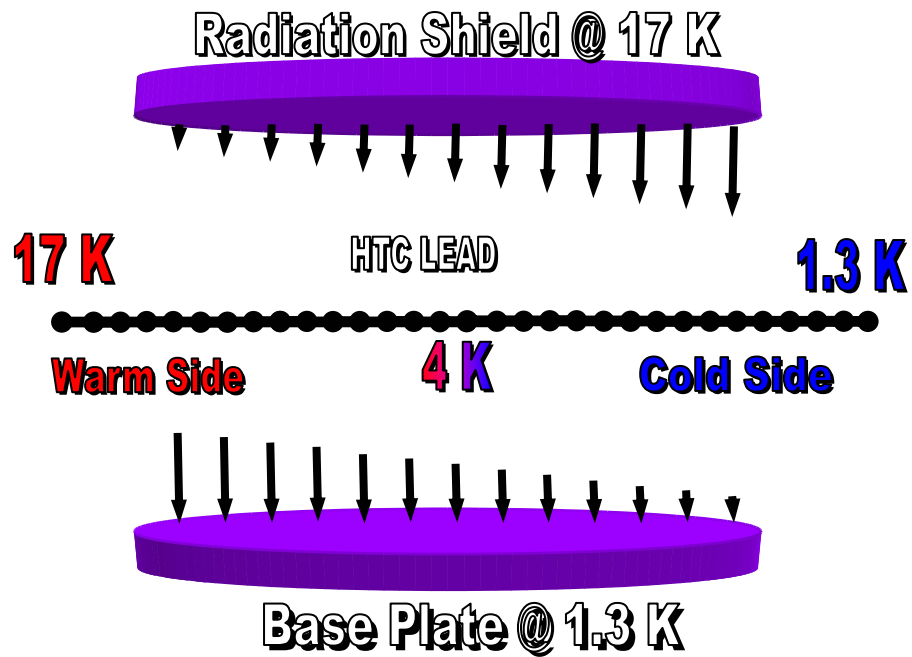
Figure 4.4. Model Schematic

An energy balance is applied at each of the nodes to calculate the heat flow as shown in Figure 4.5.
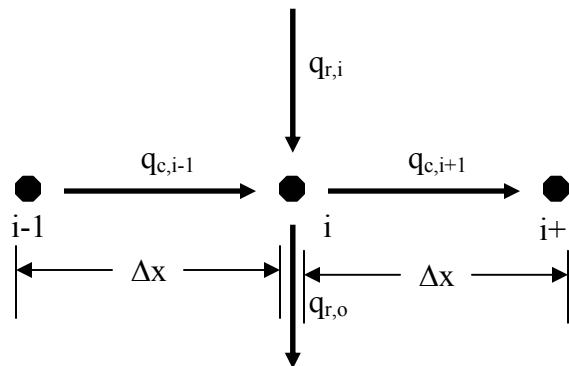
Figure 4.5. Energy Balance in a Single Node

The heat flow balance in one single node can be expressed as

$$q_{c,i-1} + q_{r,i} = q_{c,i+1} + q_{r,o} \quad\quad\quad\text{(4.12)}$$

where the heat flow in each section is defined as

$$q_{c,i-1} = k_{i-1} A \left(\frac{T_i - T_{i-1}}{\Delta x} \right) \quad\quad\quad\text{(4.13)}$$

$$q_{c,i+1} = k_{i+1} A \left(\frac{T_{i+1} - T_i}{\Delta x} \right) \quad\quad\quad\text{(4.14)}$$

$$q_{r,i} = \varepsilon \sigma A \left(T_i^4 - T_{17K}^4 \right) \quad\quad\quad\text{(4.15)}$$

$$q_{r,o} = \varepsilon \sigma A \left(T_{1.3K}^4 - T_i^4 \right) \quad\quad\quad\text{(4.16)}$$

In the 4 K heat sink node, another term is added to be able to calculate the heat going out to the heat sink. An energy balance at the 4 K node is shown in Figure 4.6.
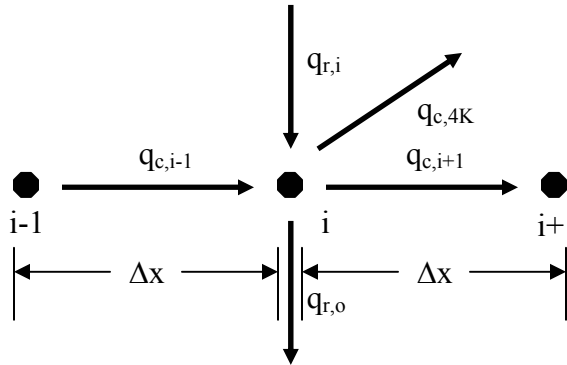
Figure 4.6. Energy Balance in the 4 K Heat Sink Node

The heat flow balance in the 4 K heat sink node can be expressed as

$$q_{c,i-1} + q_{r,i} = q_{c,i+1} + q_{r,o} + q_{c,4K} \qu\quad\quad\text{(4.17)}$$

where the heat flow in each section is defined by Equations 4.13 to 4.16.

Once the equations were defined, they were solved at each node using the Engineering Equation Solver (EES) package [22]. EES uses a variation of Newton's method [23-25] to solve systems of non-linear algebraic equations. The Jacobian matrix needed in Newton's method is evaluated numerically at each iteration.

Sparse matrix techniques [26-28] are employed to improve the calculation's accuracy and allow rather large problems to be solved. The accuracy and convergence properties of the solution method are further improved by the step-size alteration and implementation of the Tarjan [29] blocking algorithm which breaks the problems into smaller problems which are easier to solve. Several algorithms are implemented to determine the minimum or maximum value of a specified variable [30]. Even though, it looks like a set of simultaneous equations, it is often possible to solve these equations in groups (sometimes one at the time) rather than all together as one set. Solving equations in groups makes Newton's method work more efficiently. For this reason, EES organizes the equations into groups (or blocks) before solving.

EES has the capability of finding the minimum or maximum value of a variable when there is one to ten degrees of freedom. For problems with a single degree of freedom, EES can use either of two basic algorithms to find a minimum or maximum: a recursive quadratic approximation known as Brent's method or a Golden Section search [9]. For this investigation, the Brent's method was used to optimize the design in terms of the location of the 4 K heat sink.

On the other hand, EES has a user interface or diagram window feature where the user can draw a schematic that represent what is being modeled. Figure 4.5 shows a

single schematic for one wire where the user can change the warm and cold temperature and the cold and total length for the wire. This user interface was very useful to develop the diagram in order to validate the model.
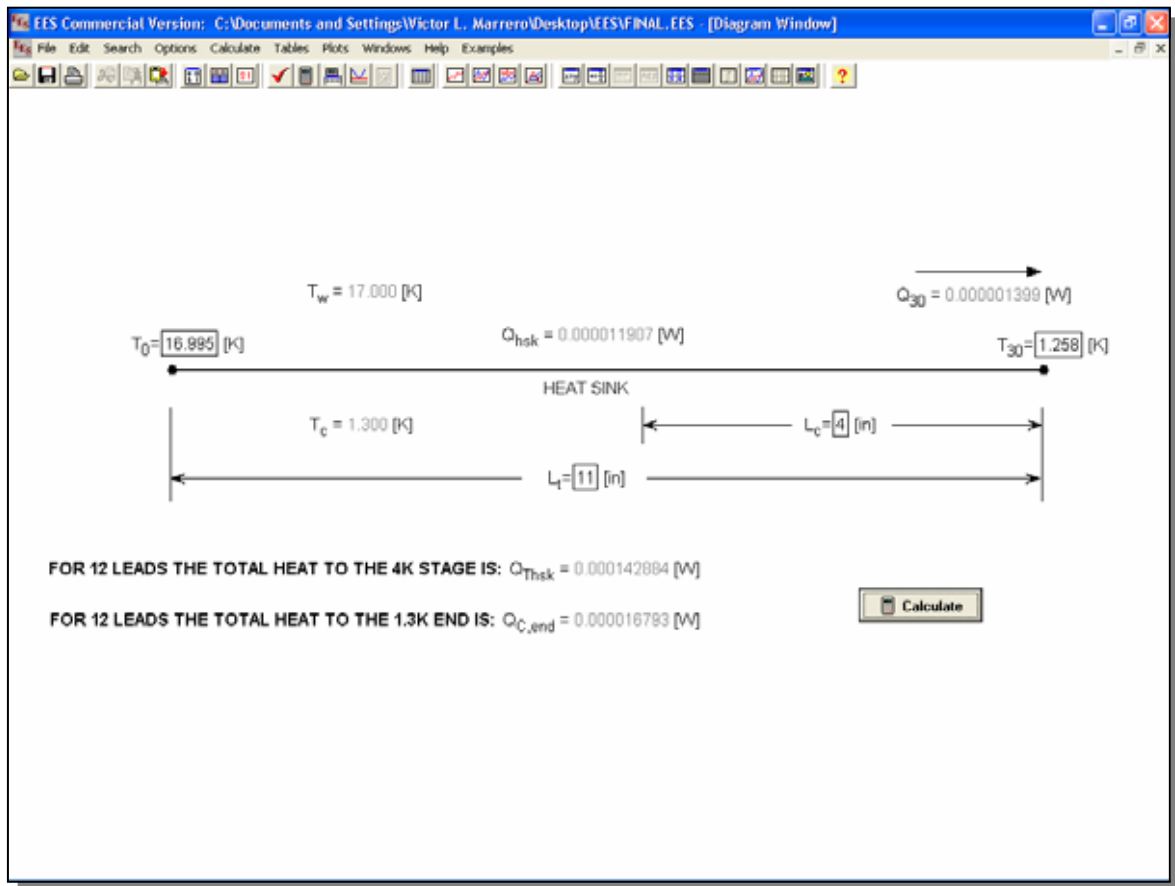
Figure 4.7. EES Diagram for a Single Prototype Wire

In summary, the thermal model developed provides the user the capability to changing: assembly dimensions, boundary temperature conditions, and locations of the heat sink. With some modifications of the code, the model can simulate more than one heat sink in the assembly.

CHAPTER 5

RESULTS AND DISCUSSIONS

Once the computer model was developed and setup, the experimental values were used to calibrate and validate the model, Table 5.1. The model was used to evaluate and optimize the design with the MgB_2 properties. The location of the joint was analyzed to minimize the heat loads into the 1.3 K and 4 K stages.

Stage	Power Need without Prototype	Temperature Read	Power Need with Prototype	Temperature Read	Total Power Transfer
17 K	78 μW	17.0049 K	204 μW	17.0052 K	+ 126 μW
4 K	1,281 μW	3.9994 K	1,142 μW	4.002 K	- 139 μW

Table 5.1. Power Need to Keep Steady Temperature in Each Stage

The emissivity of the PTFE was varied from zero to one; where zero is no radiation and one is black body behavior. This variation was done due to the lack of information of the emissivity for the PTFE at this temperature range. By solving the energy balance equations, the model predicted a heat load in the 4 K heat sink stage of 135 μW ($\varepsilon=0$) and 143 μW ($\varepsilon=1$), as shown in Figure 5.1. The model output showed an error of a 2.9% between the experimental value in the 4 K heat sink stage of 139 μW and the emissivity boundaries in the model. This error was within acceptable margins to considered the model validated. Now it can be used with confidence to make an

optimization for the MgB$_2$ HTSC lead assembly. Once the model was validated, it was used to run three different cases.

Case #1. Prediction and optimization of the 4 K heat sink location for the MgB$_2$ assembly.

Case #2. New temperature conditions on the cold and warm side.

Case #3. Prediction of the optimal location for running two heat sinks at 10 K and 4 K, respectively.

Case #1

The goal of this case was the determination of the optimal position for the 4 K heat sink to minimize the heat load into the cryostat. One parameter that was changed in the model was the thermal conductivity. The value used in the final assembly was different from the one in the prototype, because the MgB$_2$ material. Additionally, the heat sink location was calculated to minimize the heat load into the cryostat. Different thermal conductivity tests were made to early samples of the MgB$_2$ wires revealed that the conductivity of MgB$_2$ can be approximated to three times the conductivity of Stainless Steel. During the first HTSC design it was found that for every 100 μW input to the 4 K stage, 14.5 μW were added to the He tank [1]. Therefore the equation to be minimized was,

$$\dot{Q}_T = Q_{1.3K} + 0.145 Q_{4KHsk} \tag{5.1}$$

To minimize Equation 5.1 the location of the 4 K heat sink, using MgB$_2$, was 3.45 inches from the cold end, Figure 5.1. For practical purposes the location of the heat sink

was chosen at 3.5 inches. At this location, the model predicted a total heat flowing into the He tank of 169.5 µW. This calculation was done assuming the worst case scenario, where the wire is considered a black body. Therefore, this result could be interpreted as the maximum expected heat load into the He tank.
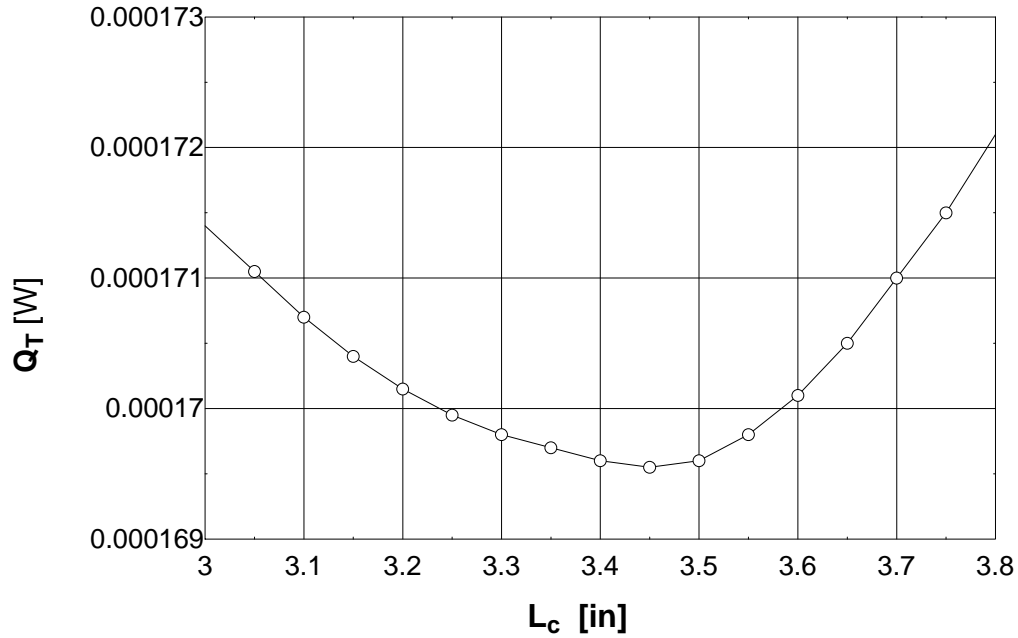
Figure 5.1. 4 K Heat Sink Location Optimization

Using the same configuration of the SS316 prototype and changing the conductivity for the MgB$_2$, the model predicts a total heat load into the Cryostat of 167.4 µW (ε=0) and 169.8 µW (ε=1), as shown in Figure 5.2. The power needed at the 4 K heat sink stage was 860 µW (ε=0) and 867 µW (ε=1), as shown in Figure 5.3. The model's predictions at the 1.3 K stage were 42.6 µW (ε=0) and 44 µW (ε=1), as shown in Figure 5.4.
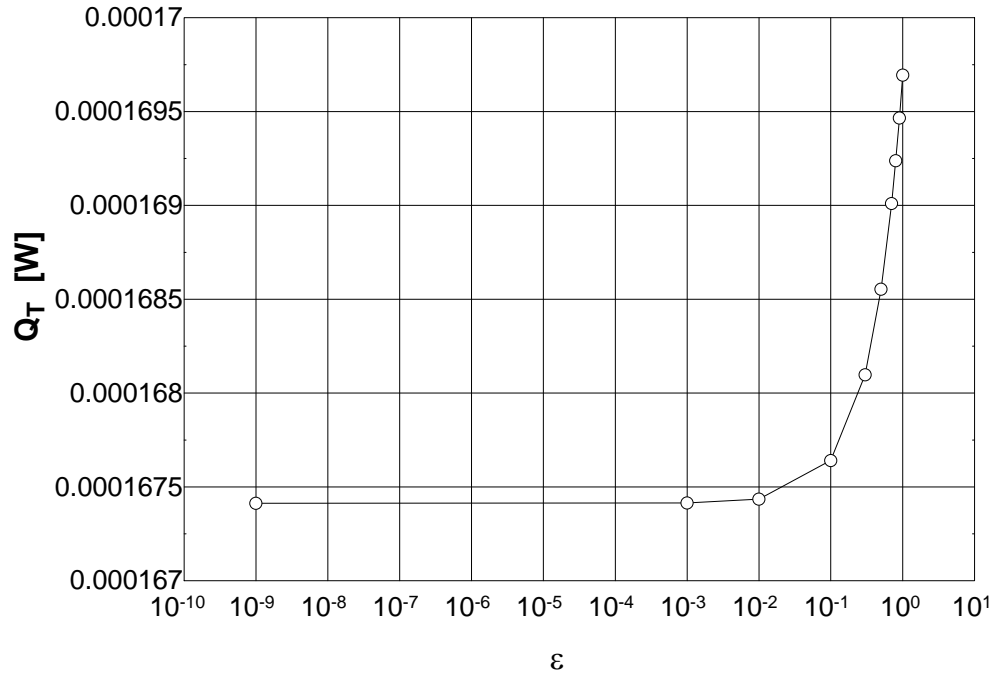
Figure 5.2. Model Prediction of Total Heat Load for the MgB$_2$ at the Cryostat for $0 \leq \varepsilon \leq 1$
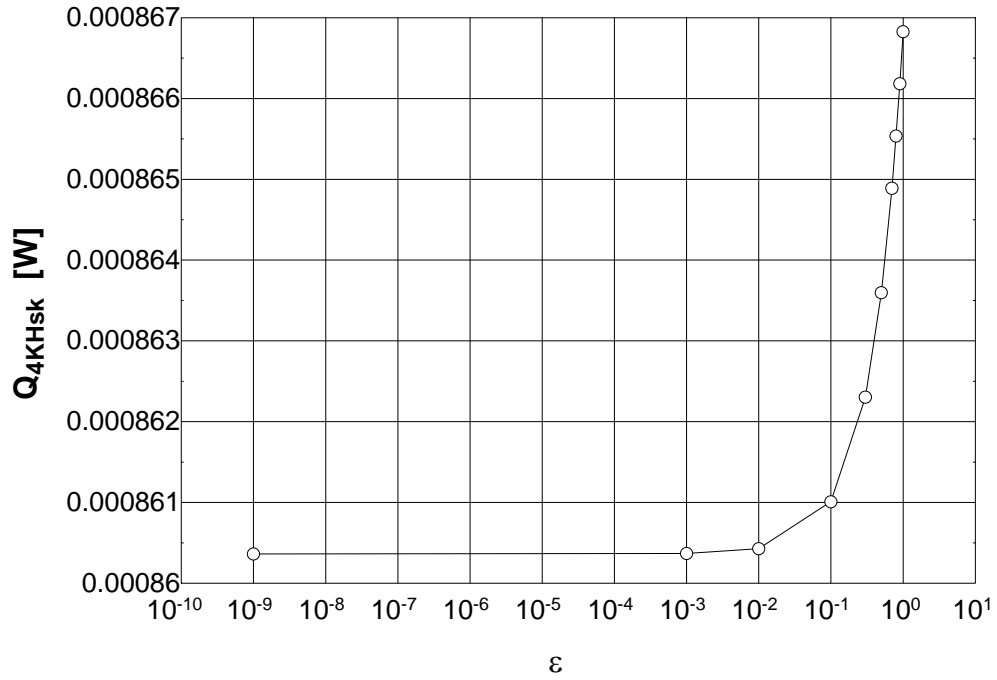
Figure 5.3. Model Prediction of the Heat Sink for the MgB$_2$ at the 4 K Stage for $0 \leq \varepsilon \leq 1$

The modeling results at each stage are summaries and compare with the experimental values as shown in Table 5.2.

Stage	Experimental	Model	Error %
1.3 K	36 μW	42.6 μW (ε=0)	18% (ε=0)
		44 μW (ε=1)	22% (ε=1)
4 K	870 μW	860 μW (ε=0)	-1.15% (ε=0)
		867 μW (ε=1)	-0.34 % (ε=1)

Table 5.2. Final HTSC Lead Assembly Modeling Results

The model underestimated the warm side of the assembly, but overestimated the cold side experimental values. This could be due to the conductivity function used in the model. The thermal conductivity function was obtained by experimentation of early tests with MgB$_2$ wires and was not calibrated for the entire temperature range.
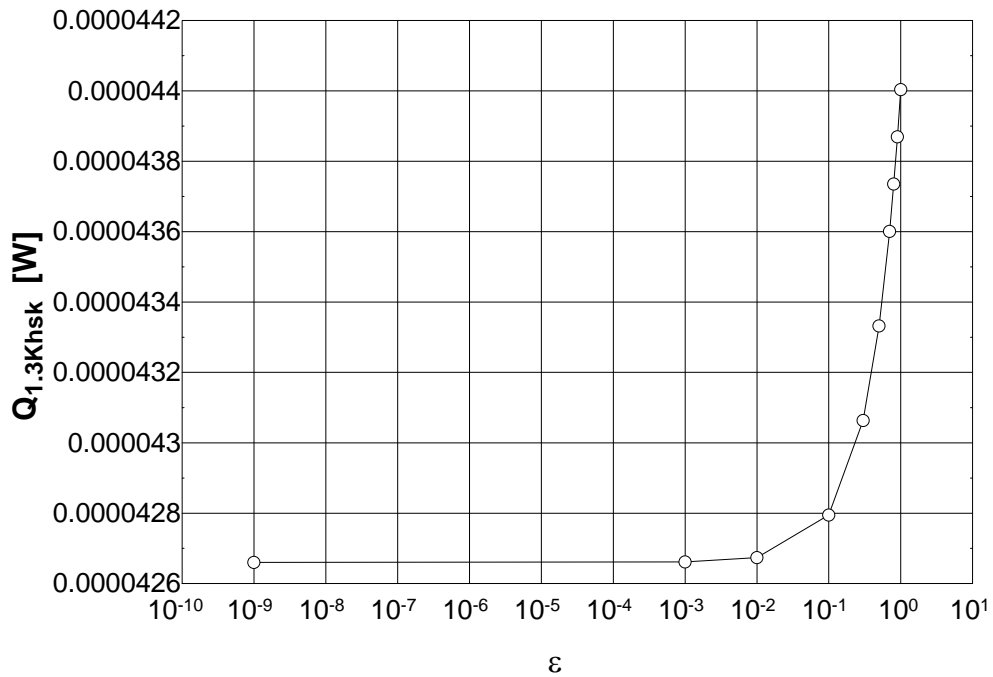
Figure 5.4. Model Prediction of the Heat Sink for the MgB$_2$ at the 1.3 K Stage for $0 \leq \varepsilon \leq 1$

Case #2

The objective of this case was to calculate the thermal loads of the assembly under different environmental conditions. There are possibilities that the Neon tank in XRS could run 1 K higher or lower from its design temperature of 17 K. On the other hands, the He tank can run low as 1.1 K, instead of 1.3 K. It is of interest to know the prediction of the thermal performance of the HTSC leads under these conditions. These results could be used in the prediction of the lifetime of the aircraft in case these conditions would prevail. The following figures show the total thermal load, 4 K stage and 1.3 stage loads for four scenarios. Figure 5.5-5.7 shows the results for Ne at 16 K and LHe at 1.3 K. Figure 5.8-5.10 shows the results for the Ne at 16 K and LHe at 1.1 K. Figure 5.11-5.13 shows the results for Ne at 18 K and LHe at 1.3 K and, Figure 5.14-5.16 shows the results for the Ne at 18 K and LHe at 1.1 K.
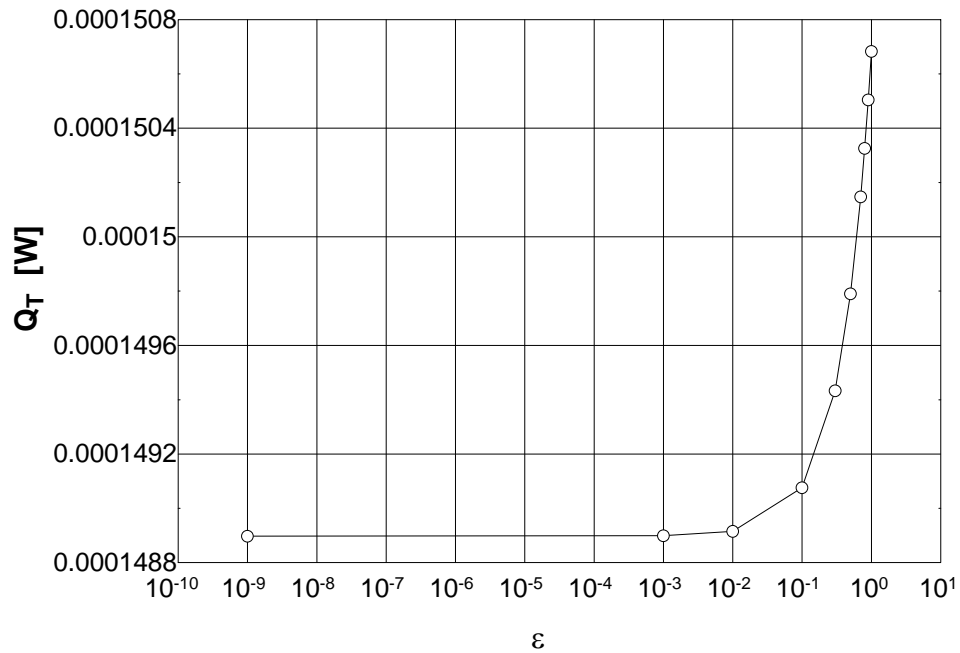
Figure 5.5. Model Prediction of the Total Heat Load when Ne tank is at 16 K and the Cryostat at 1.3K for $0 \leq \varepsilon \leq 1$

65
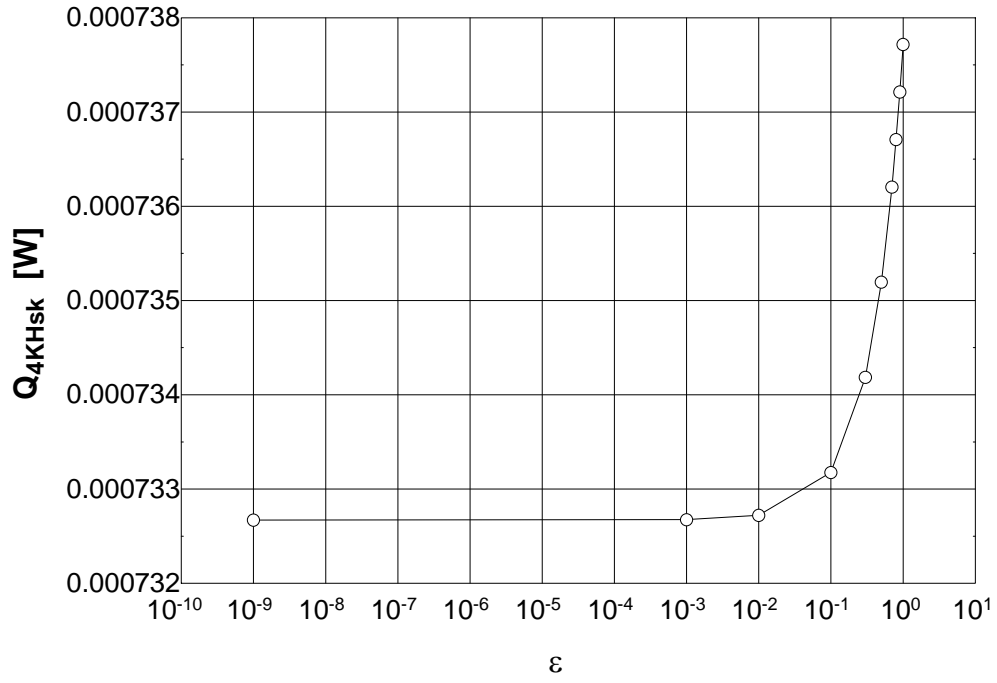
Figure 5.6. Model Prediction of the 4 K Heat Sink Load when Ne tank is at 16 K and the Cryostat at 1.3K for $0 \leq \varepsilon \leq 1$
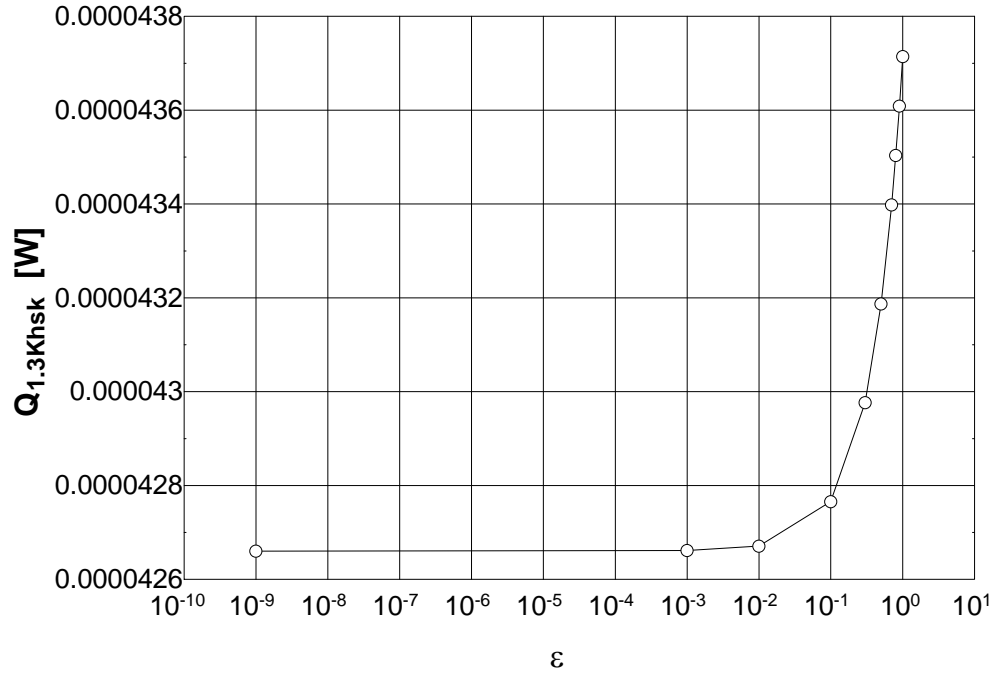
Figure 5.7. Model Prediction of the 1.3 K Heat Sink Load when Ne tank is at 16 K and the Cryostat at 1.3K for $0 \leq \varepsilon \leq 1$
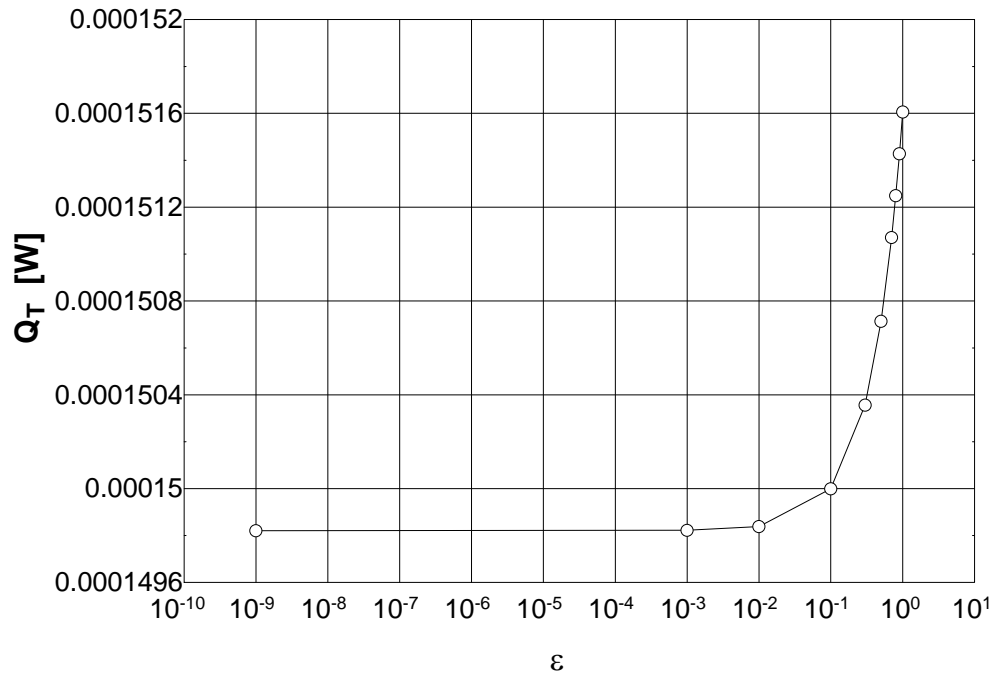
Figure 5.8. Model Prediction of the Total Heat Load when Ne tank is at 16 K and the Cryostat at 1.1K for $0 \leq \varepsilon \leq 1$
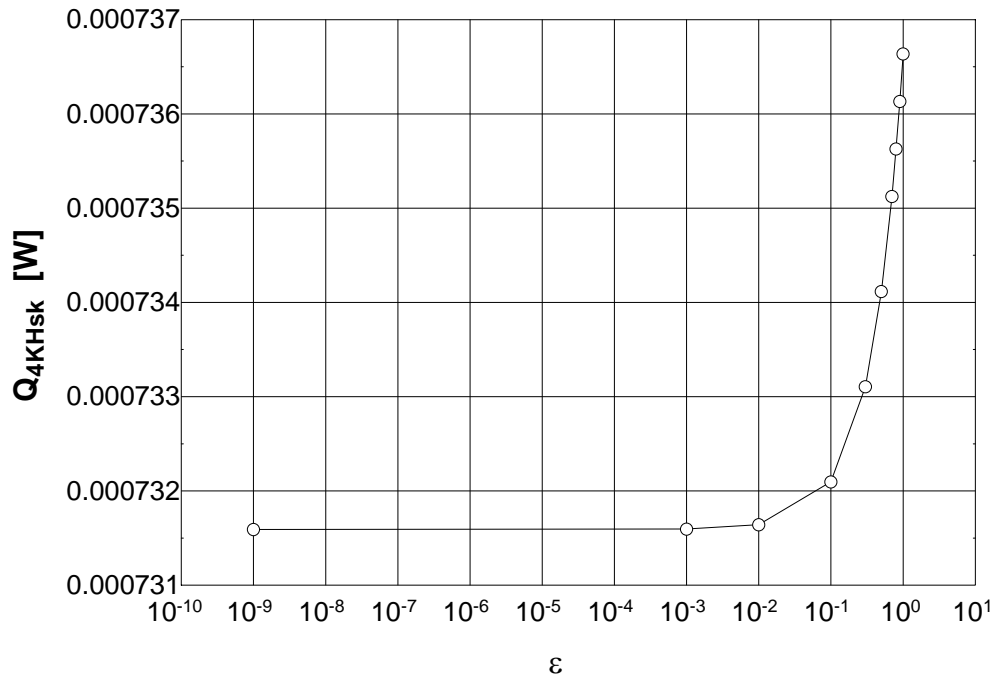
Figure 5.9. Model Prediction of the 4 K Heat Sink Load when Ne tank is at 16 K and the Cryostat at 1.1K for $0 \leq \varepsilon \leq 1$
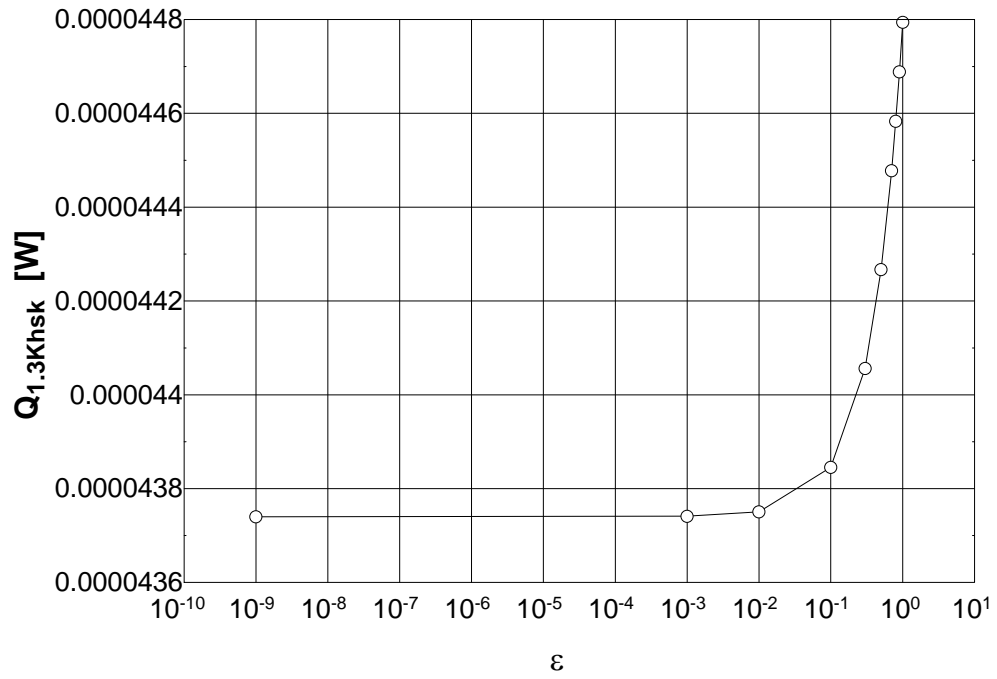
Figure 5.10. Model Prediction of the 1.3 K Heat Sink Load when Ne tank is at 16 K and the Cryostat at 1.1K for $0 \leq \varepsilon \leq 1$
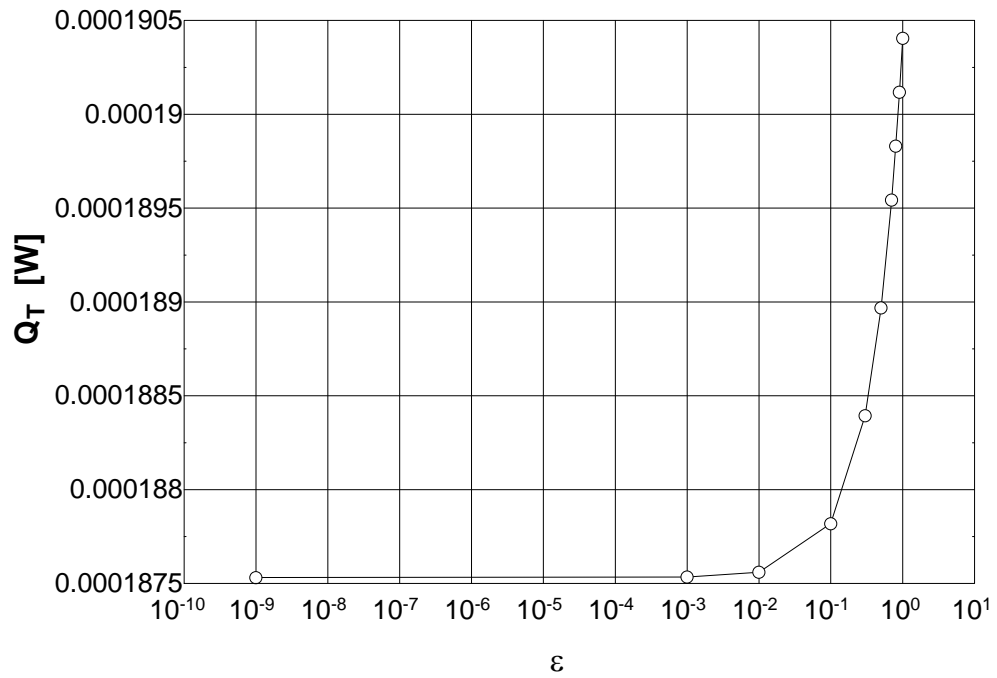
Figure 5.11. Model Prediction of the Total Heat Load when Ne tank is at 18 K and the Cryostat at 1.3K for $0 \leq \varepsilon \leq 1$
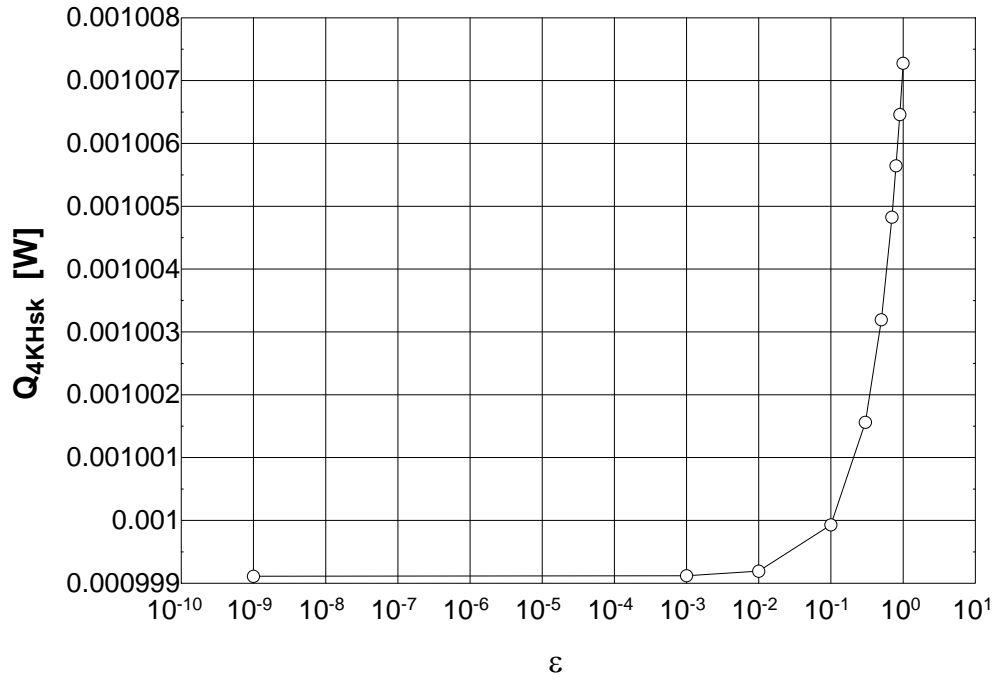
Figure 5.12. Model Prediction of the 4 K Heat Sink Load when Ne tank is at 18 K and the Cryostat at 1.3K for $0 \leq \varepsilon \leq 1$
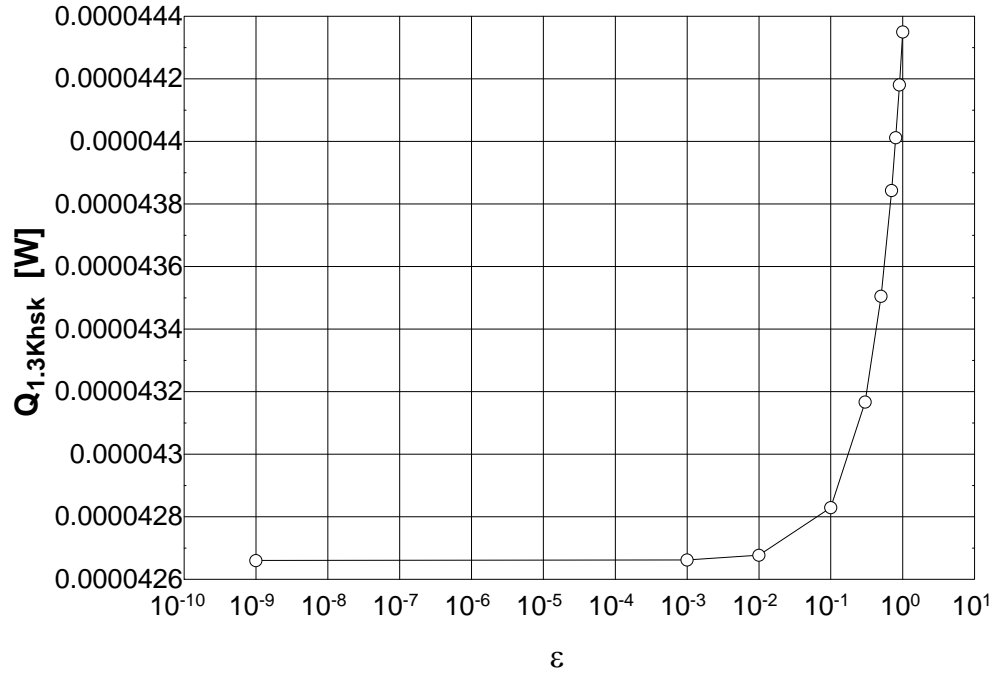
Figure 5.13. Model Prediction of the 1.3 K Heat Sink Load when Ne tank is at 18 K and the Cryostat at 1.3K for $0 \leq \varepsilon \leq 1$
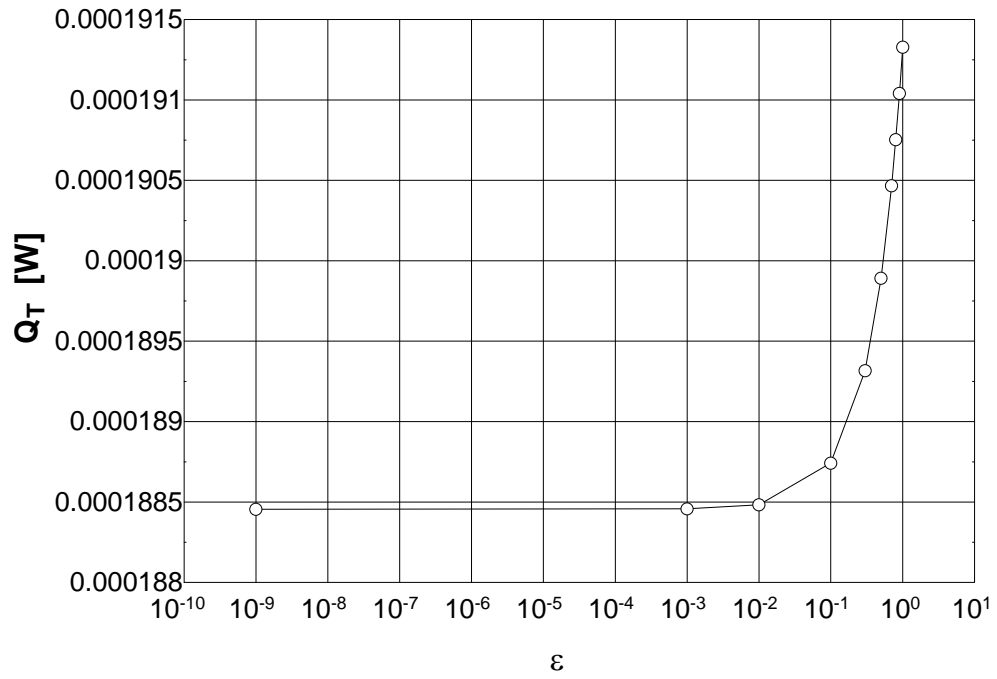
Figure 5.14. Model Prediction of the Total Heat Load when Ne tank is at 18 K and the Cryostat at 1.1K for $0 \leq \varepsilon \leq 1$
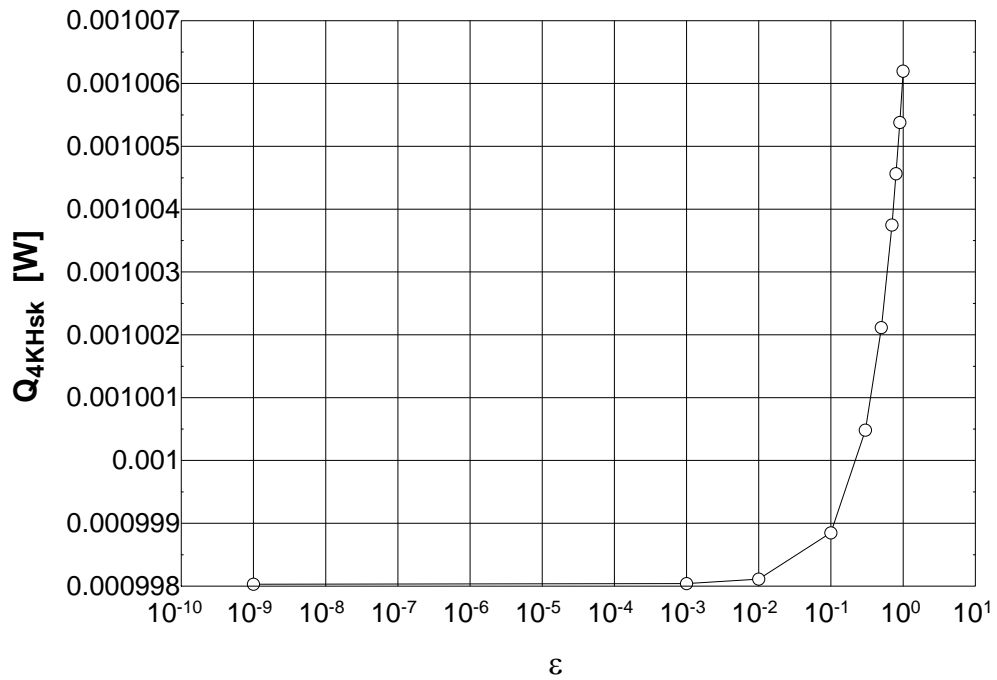
Figure 5.15. Model Prediction of the 4 K Heat Sink Load when Ne tank is at 18 K and the Cryostat at 1.1K for $0 \leq \varepsilon \leq 1$

0.0000456

0.0000452

0.0000448

$Q_{1.3Khsk}$ [W]

0.0000444

0.000044

0.0000436

10^{-10} 10^{-9} 10^{-8} 10^{-7} 10^{-6} 10^{-5} 10^{-4} 10^{-3} 10^{-2} 10^{-1} 10^{0} 10^{1}

ε
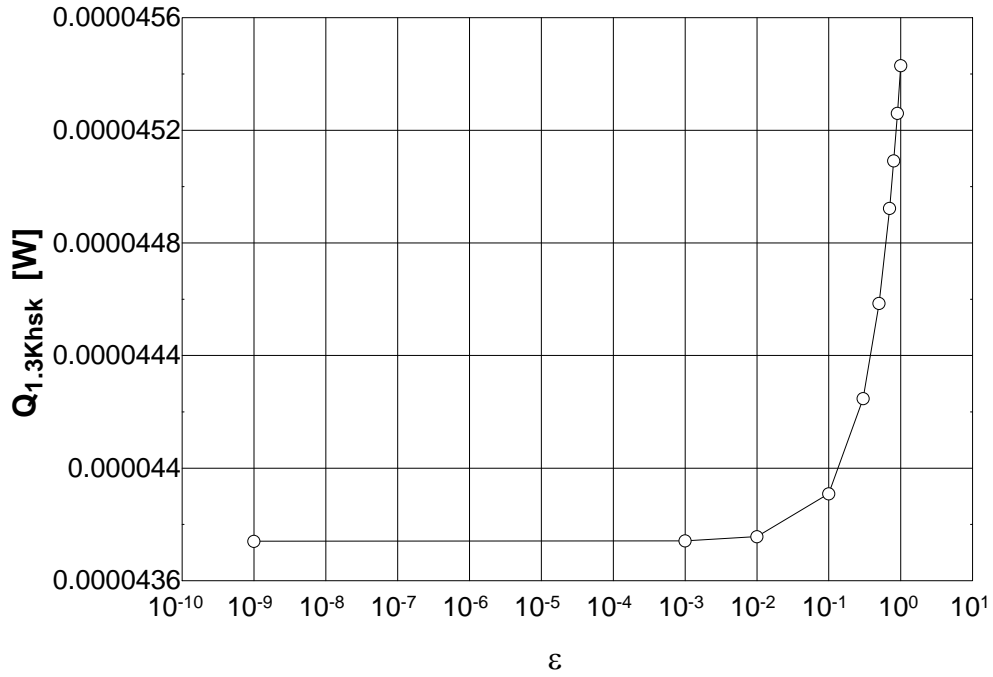
Figure 5.16. Model Prediction of the 1.3 K Heat Sink Load when Ne tank is at 18 K and the Cryostat

at 1.1K for $0 \leq \varepsilon \leq 1$

The model outputs presented graphically in the previous figures is summarized in Table 5.3. The model predicts that the worst case scenario for the XRS is if the Neon tank runs at 18 K and the Cryostat at 1.1 K at the same time. On the other hand, if the Neon tank runs at 18 K and the Cryostat at 1.3 K, at the same time, the model predicts a lower heat load compared with the actual design.

Scenario		Total Heat Load		4 K Heat Load		1.3 K Heat Load	
Neon	Cryostat	Min	Max	Min	Max	Min	Max
16 K	1.3 K	149 μW	150 μW	732.5 μW	737.5 μW	42.7 μW	43.7 μW
16 K	1.1 K	149.8 μW	151.6 μW	731.5 μW	736.5 μW	43.7 μW	44.8 μW
18 K	1.3 K	187.5 μW	190 μW	999 μW	1007 μW	42.7 μW	44.3 μW
18K	1.1 K	188.5 μW	191 μW	998 μW	1006 μW	43.7 μW	45.4 μW

Table 5.3. Model Outputs for the Case #2 Configurations

Case #3

Since the thermal load to the cryostat is higher compared to the first HTSC assembly, new configurations were studied. Thus, the main objective of this run was to calculate the optimal positions for a 10 K and a 4 K heat sinks. Calculations yield a contribution for each heat sink to the cryostat would be 7.14% and 1%, for the 4 K and 10 K, respectively. Table 5.3 summaries the thermal load at each heat sink and the total contribution to the cryostat (Equation 5.2).

$$\dot{Q}_T = Q_{1.3K} + 0.0714 Q_{4KHsk} + 0.01 Q_{10KHsk} \tag{5.2}$$

Based on the model outputs (Table 5.4) the optimal configuration is obtained when the cold side is at 4 in, cold-warm at 3 in, and the warm at 2 in. In this configuration the total heat load to the cryostat is 81 μW. It is evident that this configuration is much better than the heat sink configuration that predicted a total of 131.2 μW to the cryostat.

In summary, three different scenarios at which the HTSC assembly could be exposed, were included in this chapter. Based on the results obtained by the modeling, the best configuration to increase the lifetime of the spacecraft is when two heat sinks are used. Verification must be made to check that this thermal configuration can be implemented without any disturbance with any other parts of the spacecraft. On the other hand, vibration analysis must be performed to qualify the design for basic requirements.

L_c (in)	L_{cw} (in)	L_w (in)	Q_{10KHsk} (W)	Q_{4KHsk} (W)	$Q_{1.3K}$ (W)	Q_T (W)
1	1	7	-0.0007199	0.001107	0.00014943	0.0002213
1	2	6	-3.439E-06	0.0004814	0.00014943	0.0001838
1	3	5	0.0003302	0.0002737	0.00014943	0.0001723
1	4	4	0.0006212	0.0001706	0.00014943	0.0001678
1	5	3	0.0009941	0.0001092	0.00014943	0.0001672
1	6	2	0.001655	0.00006876	0.00014943	0.0001709
1	7	1	0.003542	0.00004027	0.00014943	0.0001877
2	1	6	-0.000632	0.001182	7.5266E-05	0.0001534
2	2	5	0.0001199	0.0005566	7.5266E-05	0.0001162
2	3	4	0.0005154	0.0003489	7.5266E-05	0.0001053
2	4	3	0.0009301	0.0002457	7.5266E-05	0.0001021
2	5	2	0.001612	0.0001844	7.5266E-05	0.0001046
2	6	1	0.003511	0.0001439	7.5266E-05	0.0001207
3	1	5	-0.0005086	0.001208	0.00005087	0.000132
3	2	4	0.0003051	0.0005819	0.00005087	0.00009547
3	3	3	0.0008243	0.0003742	0.00005087	0.00008583
3	4	2	0.001548	0.0002711	0.00005087	0.00008571
3	5	1	0.003468	0.0002097	0.00005087	0.0001005
4	1	4	-0.0003235	0.001221	3.8916E-05	0.0001228
4	2	3	0.000614	0.0005949	3.8916E-05	0.00008753
4	3	2	0.001443	0.0003872	3.8916E-05	0.00008099
4	4	1	0.003404	0.000284	3.8916E-05	0.00009323
5	1	3	-0.00001452	0.001229	3.1939E-05	0.0001195
5	2	2	0.001232	0.0006028	3.1939E-05	0.0000873
5	3	1	0.003298	0.0003951	3.1939E-05	0.00009313
6	1	2	0.0006038	0.001234	2.7451E-05	0.0001216
6	2	1	0.003088	0.0006083	2.7451E-05	0.0001018
7	1	1	0.002459	0.001238	2.4384E-05	0.0001374

Table 5.4. Model Outputs for the Two Heat Sink Configuration

CHAPTER 6

CONCLUSIONS

The research work presented consisted on the redesign of the original ASTRO-E HTSC leads, to provide a better margin of safety to the entire mission. The design parameters in this work were mainly related to the thermal performance of the HTSC leads, in particular to the amount of heat conducted along the system. Some of the conclusions obtained from this investigation are summarized as follows.

- The final HTSC lead assembly was developed using the recent discovered superconducting Magnesium Diboride (MgB_2). A thermal test was performed successfully and the data obtained was compared with the model outputs. The comparison shows that the model under-predicted the warm side and over predicted the cold side of the assembly. This difference could be due to the fact that the thermal conductivity used in the model was based on early samples of the MgB_2 wires and the final assembly. The final assembly was made on a next generation wire that was developed in a different manner. This could explain a different thermal conductivity, and therefore, an error between the model and the experimentation.

- During the model validation, the overall error between the model and the experimentation was around 2.9%. The experimental values used for validation the model were the stainless steel 316 prototype.

- Three different scenarios were simulated to study the thermal loads of the assembly under different system operation condition. The first scenario consisted of the optimization of the design to decrease the thermal load and to find the optimal position for the 4 K heat sink. The second scenario presented the thermal behavior of the system under different temperature conditions for the cold and warm end. Finally, the third scenario consisted of the evaluation of the implementation of two heat sinks at 10 K and 4 K, respectively. The conclusions obtained after analyzing the results of the thermal behavior of the systems under the different conditions are summarized as follows.

  * Case #1: the model predicted an optimal position of 3.5 inches from the cold side, for the 4 K heat sink to decrease the thermal load into the cryostat. In this position the model predicts 867 µW for the 4 K heat sink, 44 µW for the 1.3 K cold side and a total heat load on the cryostat of 169.5 µW.

  * Case #2: the model predicted (Table 5.3) a worst and a best case scenario of the thermal load into the cryostat when the Neon and Helium tanks are operating at different design temperatures. The worst case scenario was predicted to be a thermal load of 188.5 µW when the Neon tank is running at 18 K and the Helium tank at 1.1 K. This is a 12% increase in the thermal load into the cryostat compared to the normal operation of 17 K and 1.3 K for the Neon and Helium tank, respectively. The model predicted the best scenario to be a thermal load of 149 µW to the cryostat when the Neon tank

is at 16 K and the Helium tank at 1.3 K. This represents an 11% decrease in the thermal load into the cryostat compared to normal operational conditions.

* Case # 3: the model outputs predicted an optimal configuration for two heat sinks at 10 K and 4 K when the cold side is 4 in, cold-warm 3 in, and the warm 2 in long. In this configuration the total heat load to the cryostat was predicted to be 81 μW. It is evident that this configuration is much better than the one-heat sink configuration, which predicted a total of 131.2 μW to the cryostat.

In conclusion, it was observed that in order to decrease the heat load into the cryostat, the best configuration for the HTSC leads is when it has two heat sinks at 10 K and 4 K, respectively. In order to implement this design, verification must be made to assure that this configuration does not create a thermal short in any other parts of the spacecraft when employed in vibration testing. Additionally, it is recommended to develop and use MgB_2 wire with smaller diameter to decrease the total heat load. By changing the wire diameter, it implies that the PTFE tubing will be smaller, resulting in a lower mass assembly. This is needed, because the addition of a second heat sink will increase the total weight and, therefore lower the resonance frequency of the assembly.

Finally, the development and validation of the thermal model for the HTSC leads can benefits future designs. During the design process it could be used as a tool to optimize the design and evaluate different scenarios. It can be modified to employed more heat sinks and consider different materials.

BIBLIOGRAPHY

[1] Tuttle, J.G., T.P. Hait, R.F. Boyle, H.J. Muller, J.D. Hodge, and S.R. Breon, "A High Tc Superconducting Current Lead Assembly for the XDS Helium Cryostat", *Advances in Cryogenics Engineering, 43, pp. 965-972, 1998*

[2] Diaz A., and R. Kelly, "Astro-E2 Phase A Report", *NASA/GSFC Code 552, 2001*

[3] Breon, S.R., P. Shirron, R. Boyle, E. Canavan, M. Di Pirro, A. Serlemitsos, J. Tuttle, and P. Whitehouse, "The XRS Low Temperature Cryogenic System: Ground Performance Test Results", *Cryogenics, 39, pp. 677-690, 1999*

[4] Boyle, R., "XDS Thermal Anomaly Summary", *NASA/GSFC Code 552, 2001*

[5] Wilson, M.N, "Superconducting Magnets", *Clarendon Press – Oxford, Chapter 11, 1990, ISBN 0-19-854805-2*

[6] Seol, S.Y., Y.S. Cha, R.C. Niemann, and J.R. Hull, "Prediction of Burnout of a Conduction-Cooled BSCCO Current Lead", *IEEE Transactions on Applied Superconductivity, 7, pp. 696-699, 1997*

[7] Malinowski, L., "Explicit Expression for Critical Energy of Uncooled Superconductors Considering Transient Heat Conduction", *Cryogenics, 39, pp. 311-317, 1999*

[8] Citver, G., E. Barzi, A. Burov, S. Feher, P.J. Limon, and T. Peterson, "Steady State and Transient Current Lead Analysis", *IEEE Transactions on Applied Superconductivity, 9, pp. 515-518, 1999*

[9] Ünal, A., and M.-C. Chyu, "Instability Behaviour of Superconductor Wires/Cylinders under Finite Linear Thermal Disturbance", *Cryogenics, 35, pp. 87-92, 1995*

[10] Koizumi, N., Y. Takahashi, and H. Tsuji, "Numerical Model using an Implicit Finite Difference Algorithm for Stability Simulation of a Cable-in-Conduit Superconductor", *Cryogenics, 36, pp. 649-659, 1996*

[11] Flik, M.I., P.E. Phelan, and C.L. Tien, "Thermal Model for the Bolometric Response of High Tc Superconducting Films to Optical Pulse, *Cryogenics, 30, pp. 1118-1128, 1990*

[12] Phelan, P.E., "Thermal Response of Thin-Film High-Tc Superconductors to Modulated Irradiation", *Journal of Thermophysics and Heat Transfer, 9, pp. 397-402, 1995*

[13] Koo, J.M., and S. Park, "Thermal Analysis on Voltage Response of High-Tc Superconducting Thin-Films Exposed to a Pulse Laser Beam", *KSME International Journal, 12, pp. 143-152, 1998*

[14] Malinowski, L., "Novel Model for Evolution of Normal Zones in Composite Superconductors", *Cryogenics, 33, pp. 724-728, 1993*

[15] Lewandowska, M., and L. Malinowski, "Analytical Method for Determining Critical Energies of Uncooled Superconductors based on the Hyperbolic Model of Heat Conduction", *Cryogenics, 41, pp. 267-273, 2001*

[16] Lor, W., and H. Chu, "Hyperbolic Heat Conduction in Thin-Film High Tc Superconductors with Interface Thermal Resistance", *Cryogenics, 39, pp. 739-750, 1999*

[17] Al-Odat, M., M.A. Al-Nimr, and M. Hamdan, "Superconductor Thermal Stability under the Effect of the Dual-Phase-Lag Conduction Model", *International Journal of Thermophysics, 23, pp. 855-868, 2002*

[18] Nagamatsu J., N. Nakagawa, T. Muranaka, Y. Zenitani, and J. Akimitsu, "Super-conductivity at 39 K in Magnesium Diboride", *Nature, 410, pp. 63-64, 2001*

[19] Schlachter S., W. Goldacker, J. Reiner, S. Zimmer, B. Liu, and B. Obst, "Influence of Preparation Process in Microstructure, Critical Current Density and Tc of MgB_2 Powder-in-Tube Wires", *Manuscript, August 2002*

[20] Kumakura H., A. Matsumoto, H. Fujii, K. Togano, "High Transport Critical Current Density Obtained for Powder-In-Tube-Processed MgB_2 Tapes and Wires Using Stainless Steel and Cu-Ni Tubes", *Manuscript, 2001*

[21] Pobell F., "Matter and Methods at Low Temperatures", *Springer, pp. 54-108, 1996, ISBN 3-540-58572-9*

[22] Klein S.A. and F.L. Alvarado, "Engineering Equation Solver (EES) User Manual", *F-Chart Software, www.fchart.com, 2002*

[23] Al-Khafaji, A. W. and J.R. Tooley, "Numerical Methods in Engineering Practice", *Holt, Rinehart and Winston, 1986*

[24] Gerald, C.F. and P.O. Wheatley, "Applied Numerical Analysis", *Addison-Wesley, 1984*

[25] Ferziger, J.H., "Numerical Methods for Engineering Application", *Wiley-Interscience, 1981*

[26] Duff, I.S., A.M. Erisman, and J.K. Reid, "Direct Methods for Sparce Matrices", *Oxford Science Publications, Clarendon Press, 1986*

[27] Pissanetsky, S., "Sparse Matrix Technology", *Academic Press, 1984*

[28] Alvarado, F.L., "The Sparse Matrix Manipulation System", *Report ECE-89-1, Department of Electrical and Computer Engineering, The University of Wisconsin, Madison, 1989*

[29] Tarjan, R., "Depth-First Search and Linear Graph Algorithms", *SIAM J. Comput. 1, pp. 146-160, 1972*

[30] Press, W.H., B.P. Flannery, S.A. Teukolsky, and W.T. Vetterling, "Numerical Recipes in Pascal", *Cambridge University Press, 1989*

[31] Wark, K., "Advanced Thermodynamics for Engineers", *McGraw-Hill, pp. 251-259, 1981*

[32] Timmerhaus K. D. and T. M. Flynn, "Cryogenic Process Engineering", *Plenum Press, ISBN 0-306-43283-8, pp. 59-76, 1989*

APPENDIX A

TECHNICAL DATA

Cernox™ RTDs

- Low magnetic field-induced errors

- High sensitivity at low temperatures and good sensitivity over a broad range

- Excellent resistance to ionizing radiation

- Fast characteristic thermal response times: 1.5 ms at 4.2 K; 50 ms at 77 K (in bare chip form in liquid)

- Broad selection of models to meet your thermometry needs

- Manufactured by Lake Shore, insuring control over wafer level quality and yield for the future

- Excellent stability

- Variety of packaging options

* Patent # 5,363,084, Nov. 1994, "Film Resistors Having Trimmable Electrodes" and 5,367,285 "Cernox™, Nov. 1994, "Metal Oxynitride Resistance Films and Methods of Making the Same," Lake Shore Cryotronics, Inc.

Cernox™ thin film resistance temperature sensors offer a negative temperature coefficient, monotonic response over a wide temperature range, low magnetic field induced errors and high resistance to ionizing radiation.

Thin film resistance temperature sensors offer significant advantages over comparable bulk or thick film resistance sensors. These new thin film sensors offer a smaller package size which makes them useful in a broader range of experimental mounting schemes and they are available in a chip form. The Cernox™ temperature sensors have proven to be very stable over repeated thermal cycling and under extended exposure to ionizing radiation. Furthermore, these thin film sensors are easily mounted in packages designed for excellent heat transfer, yielding a characteristic thermal response time much faster than possible with bulk devices requiring strain-free mounting.

Hermetic package

Canister package

Canister

Wires with the same color code are connected to the same side of the sensor. Looking at epoxy seal with leads toward user.

Typical Calibration Shifts

Typical calibration shift after 200 thermal shocks from 305 K to 77 K for a Model CX-1030 temperature sensor ($\Delta T = 1$ mK at 4.2 K and 10 mK at 100 K).

Magnetic Field Dependence
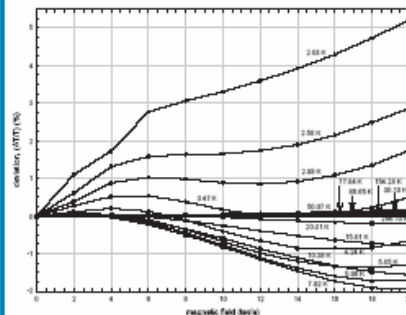
Typical temperature reading errors for operation of Model CX-1050 sensors in magnetic fields at temperatures from 2.03 K to 286 K.

See Reference Section for more information.

"Low temperature thermometry in high magnetic fields VII. Cernox™ sensors to 32 T," B. L. Brandt, D. W. Liu and L. G. Rubin; Rev. Sci. Instrum., Vol. 70, No. 1, 1999, pp 104-110.

Typical Resistance and Sensitivity values for Cernox™ RTDs. See page A-53 for tabular data.
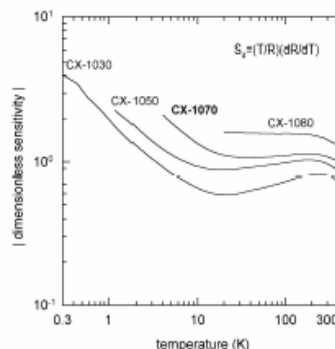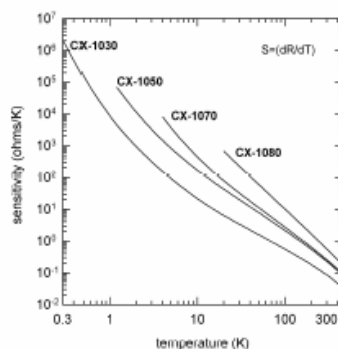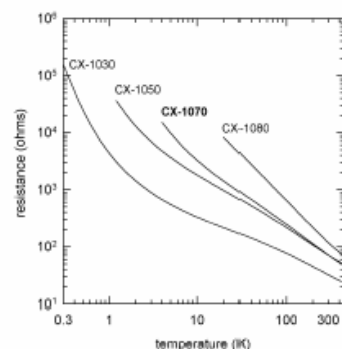
Specifications

	Unpackaged chip (BC) (BG) (BR)	Hermetic ceramic package (SD)	Copper canister package (AA) (AA)
Temperature			
Useful range			
Minimum	0.30 K (model dependent)	0.30 K (model dependent)	0.30 K (model dependent)
Maximum	325 K	325 K	325 K
Maximum storage temperature	325 K	325 K	325 K
Standard curve	Not applicable	Not applicable	Not applicable
Resistance (typical)	See plots on previous page	See plots on previous page	See plots on previous page
Sensitivity (typical)	See plots on previous page	See plots on previous page	See plots on previous page
Dimensionless sensitivity (typical)	See plots on previous page	See plots on previous page	See plots on previous page
Accuracy (interchangeability)	Not applicable	Not applicable	Not applicable
Accuracy (SoftCal™)	Not applicable	Not applicable	Not applicable
Accuracy (Calibrated)[1]	±5 mK at T < 10 K; ±20 mK at 20 K; ±35 mK at 50 K; ±140 mK at 300 K (model dependent)		
Stability[2]			
Short-term	±0.003 K at 4.2 K	±0.003 K at 4.2 K	±0.003 K at 4.2 K
Long-term	±25 mK from 1 to 100 K; 0.05% of temperature from 100 to 325 K (all models)		
Thermal response time	1.5 ms at 4.2 K / 50 ms at 77 K / 135 ms at 273 K	15 ms at 4.2 K / 0.25 seconds at 77 K / 0.8 seconds at 273 K	0.4 seconds at 4.2 K / 2 seconds at 77 K / 1.0 seconds at 273 K
Recommended recalibration schedule	Annual	Annual	Annual
Excitation			
Recommended	10 mV (1.4 to 325 K) (all models). Measurements below 1 K should be performed with an AC resistance bridge. Typical operating power is 10^{-11} W at 0.5 K[3].		
Maximum power before damage	10^{-4} W, 10 mA or 1 V continuous, whichever is less (all models)		
Dissipation at rated excitation	Typical 10^{-8} W at 300 K; 10^{-7} W at 4.2 K; 10^{-13} W at 0.3 K (model and temperature dependent)		
Units range (volts or ohms)	Typical 20 Ω at room temperature to 100,000 Ω at lower temperature limit (model dependent)		
Lead wire configuration	See lead specification below	Two lead, no polarity	Four lead, color coded
Physical Specifications – see Reference Section for more information			
Materials in the sensor construction	Ceramic oxynitride, gold pads and sapphire substrate with metallized back (chip in all models).	Chip mounted on sapphire base with alumina body and lid. Mo/Mn with nickel and gold plating on base and lid. Gold-tin solder as hermetic lid seal.	Chip mounted in a gold plated cylindrical copper can.
Size in millimeters	0.75 x 1.0 x 0.25 to 0.38 mm	3.2 mm x 1.9 mm base x 1mm	3 mm diameter x 8.5 mm long
Mass	≤3.0 milligrams	≈40 milligrams	≈400 milligrams
Leads			
Size		0.2 mm diameter x 25 mm long	0.24 mm diameter x 15 cm long
Number	BR: none; BG: two; BC: two	Two (2) (soldered attachment)	Four (4)
Material	BG: gold; BC: copper	Phosphor-bronze	32 AWG Phosphor-bronze
Insulation	BR: NA; BG: none; BC: none	None	HML Heavy Build
Internal atmosphere	Not applicable	Vacuum	Helium 4 (⁴He) is standard
Environmental – see Reference Section for more information			
Radiation effects	Recommended for use in radiation environments. See Reference Section.		
Magnetic fields	Recommended for use in magnetic fields at low temperatures. The magnetoresistance is typically negligibly small above about 30 K and not significantly affected by orientation relative to the magnetic field. Refer to plots of the temperature errors (all models).		
ESD sensitivity	Not applicable	Not applicable	Not applicable
Noise sensitivity	Not applicable	Not applicable	Not applicable

Ordering Information

Uncalibrated sensor
Specify the Model number in the left column only, for example CX-1050-SD.

Calibrated sensor
Add Calibration Range Suffix Code to the end of the Model number, for example CX-1050-SD-1.4L.

Cernox™ RTD	Calibration Range Suffix Codes Numeric figure is the low end of the calibration. Letters represent the high end: B = 40 K, D = 100 K, L = 325 K.											
Model number	0.3B	0.3D	0.3L	1.4B	1.4D	1.4L	4B	4D	4L	20B	20D	20L
CX-1020-AA	✓	✓	✓	✓	✓	✓	✓	✓	✓			
CX-1030-AA, SD, CU, LR, ET, MT,[4] BO, CO, BG, BC, CD		✓	✓	✓	✓	✓	✓	✓	✓	✓		
CX-1030-BR[4]												
CX-1050-AA, SD, CU, LR, ET, MT, BO, CO, BG, BC, CD				✓	✓	✓	✓	✓	✓	✓		
CX-1050-BR												
CX-1070-AA, SD, CU, LR, ET, MT, BO, CO, BG, BC, CD								✓	✓	✓		
CX-1070-BR												
CX-1080-AA, SD, CU, LR, ET, MT, BO, CO, BG, BC, CD										✓	✓	✓
CX-1080-BR												

Accessories suggested for installation (see Section 3):
Stycast® Epoxy   Indium Solder   Manganin Wire
Apiezon® Grease   90% Pb, 10% Sn Solder   CryoCable™
IMI-7031 Varnish   Phosphor-Bronze Wire

USD   American Express   VISA   MasterCard

(1) Bare chip sensors can only be calibrated after attaching gold wire leads. The user must remove the ball bonded leads if they are not desired. The bond pads are large enough for additional bonds.

(2) Long-term stability data is obtained by subjecting sensor to 200 thermal shocks from 305 K to 77 K. Calibration shifts are measured over the temperature range from 1.4 K to 330 K. Short-term stability data is obtained by subjecting sensor to ten thermal shocks from 305 K to 4.2 K. Data is taken at 4.2 K only.

(3) See Reference Section for self-heating information.

(4) Because the bare chips are for low temperature use (<4 K) are sorted by using 4.2 K data, there is a small probability that the actual 0.3 K resistance will be outside the published specification. If the customer requests it, Lake Shore will replace otherwise undamaged sensors.

Emerson & Cuming
a National Starch & Chemical Company

Internet Address:
www.emersoncuming.com

STYCAST® 2850 FT
Thermally Conductive Epoxy Encapsulant

Key Feature:	Benefit:
• Good thermal conductivity	• Dissipation of heat from embedded components
• Low coefficient of thermal expansion	• Low stress on embedded components

Product Description:

STYCAST 2850 FT is a two component, thermally conductive epoxy encapsulant that can be used with a variety of catalysts. It features a low coefficient of thermal expansion and excellent electrical insulative properties. The STYCAST 2850 FT Blue is recommended for use in high voltage applications where surface arcing or tracking is a concern.

Applications:

STYCAST 2850 FT is designed for encapsulation of components which need heat dissipation and thermal shock properties.

Instructions For Use:

Thoroughly read the information concerning health and safety contained in this bulletin before using. Observe all precautionary statements that appear on the product label and/or contained in individual Material Safety Data Sheets (MSDS).

To ensure the long term performance of the potted or encapsulated electrical / electronic assembly, complete cleaning of components and substrates should be performed to remove contamination such as dust, moisture, salt, and oils which can cause electrical failure, poor adhesion or corrosion in an embedded part.

Some filler settling is common during shipping or storage. For this reason, it is recommended that the contents of the shipping container be thoroughly mixed prior to use. Power mixing is preferred to ensure a homogeneous product.

Accurately weigh resin and hardener into a clean container in the recommended ratio. Weighing apparatus having an accuracy in proportion to the amounts being weighed should be used.

Blend components by hand, using a kneading motion, for 2-3 minutes. Scrape the bottom and sides of the mixing container frequently to produce a uniform mixture. If possible, power mix for an additional 2-3 minutes. Avoid high mixing speeds which could entrap excessive amounts of air or cause overheating of the mixture resulting in reduced working life.

To ensure a void-free embedment, vacuum deairing should be used to remove any entrapped air introduced during the mixing operation. Vacuum deair mixture at 1-5 mm mercury. The foam will rise several times the liquid height and then subside. Continue vacuum deairing until most of the bubbling has ceased. This usually requires 3-10 minutes. To facilitate deairing in difficult to deair materials, add 1-3 drops of an air release agent, such as ANTIFOAM 88, into 100 grams of mixture. Gentle warming will also help, but working life will be shortened.

Pour mixture into cavity or mold. Gentle warming of the mold or assembly reduces the viscosity. This improves the flow of the material into the unit having intricate shapes or tightly packed coils or components. Further vacuum deairing in the mold may be required for critical applications.

Properties of Material As Supplied:

Property	Test Method	Unit	Value
Chemical Type			Epoxy
Appearance	Visual		Black or blue liquid
Density	ASTM-D-792	g/cm³	2.35 - 2.45
Brookfield Viscosity	ASTM-D-2393 5 rpm # 7	Pa.s cP	200 - 250 200,000 - 250,000

Choice of Curing Agents			
Curing agent	Catalyst 9	Catalyst 23 LV	Catalyst 11
Description	General purpose with good chemical resistance and physical strength.	Low color, low viscosity, long pot life. Excellent, thermal shock and impact resistance. Excellent low temperature properties and adhesion to glass.	Long pot life, excellent chemical resistance, good physical and chemical properties at elevated temperatures.
Type of cure	Room	Room	Heat
Viscosity Pa.s cP	0.080 to 0.105 80 to 105	0.020 to 0.030 20 to 30	0.035 to 0.060 @ 65 °C 35 to 60 @ 65 °C

Properties of Material As Mixed:

Property	Test Method	Unit	Value		
			Catalyst 9	Catalyst 23 LV	Catalyst 11
Mix Ratio - Amount of Catalyst per 100 parts of STYCAST 2850 FT		By Weight	3.5	7.5	4.5
		By Volume	8.5	17.5	9.5
Working Life (100 g @ 25°C)	ERF 13-70		45 minutes	60 minutes	>4 hours
Density	ASTM-D-792	g/cm³	2.29	2.19	2.29
Brookfield Viscosity	ASTM-D-2393	Pa.s cP	58 58,000	5.6 5,600	64 64,000

Cure Schedule:

Cure at any one of the recommended cure schedules. For optimum performance, follow the initial cure with a post cure of 2-4 hours at the highest expected use temperature. Alternate cure schedules may also be possible. Contact your Emerson & Cuming Technical Representative for further information.

Temperature	Cure Time		
°C	Catalyst 9	Catalyst 23 LV	Catalyst 11
25	16-24 hr	16-24 hr	-
45	4-6 hr	4-6 hr	-
65	1-2 hr	2-4 hr	-
80			8-16 hr
100			2-4 hr
120			30-60 min

Properties of Material After Application:

Property	Test Method	Unit	Value		
			Catalyst 9	Catalyst 23 LV	Catalyst 11
Hardness	ASTM-D-2240	Shore D	96	92	96
Flexural Strength	ASTM-D-790	mPa	92	106	117
		psi	13,300	15,300	17,000
Compressive Strength	ASTM-D-695	mPa	155	120	193
		psi	22,500	17,400	27,900
Linear Shrinkage	ASTM-D-2566	cm/cm	0.002	0.003	0.002
Water Absorption (24 hours)	ASTM-D-570	%	0.03	0.02	0.05
Coefficient of Thermal Expansion	ASTM-D-3386				
α^1		$10^{-6}/°C$	35.0	39.4	31.2
α^2		$10^{-6}/°C$	98.9	111.5	97.9
Glass Transition Temperature	ASTM-D-3418	°C	86	68	115
Thermal Conductivity	ASTM-D-2214	W/m.K	1.25	1.02	1.28
		Btu-in/hr-ft²-°F	8.7	7.1	8.9
Temperature Range of Use		°C	-40 to +130	-65 to +105	-55 to +155
Outgassing(1)	ASTM-E-595				
TML		%	0.25		0.29
CVCM		%	0.01		0.02
Dielectric Strength	ASTM-D-149	kV/mm	14.4	14.8	15.0
		V/mil	365	375	380
Dielectric Constant @ 1 mHz	ASTM-D-150	-	5.01	5.36	5.36
Dissipation Factor @ 1 mHz	ASTM-D-150	-	0.028	0.051	0.043
Volume Resistivity @ 25°C	ASTM-D-257	Ohm-cm	$>10^{15}$	$>10^{15}$	$>10^{15}$

(1) per NASA Reference Publication 1124. Samples tested were cured for 24 hours @ 25°C using Catalyst 9, and 4 hours @ 80°C using Catalyst 11.

Storage and Handling:

The shelf life of STYCAST 2850 FT is 12 months at 25°C. For best results, store in original, tightly covered containers. Storage in cool, clean and dry areas is recommended. Usable shelf life may vary depending on method of application and storage temperature. Certain resins and hardeners are prone to crystallization. If crystallization does occur, warm the contents of the shipping container to 50-60°C until all crystals have dissolved. Be sure the shipping container is loosely covered during the warming stage to prevent any pressure build-up. Allow contents to cool to room temperature before continuing.

Health and Safety:

The STYCAST 2850 FT, like most epoxy compounds possesses the ability to cause skin and eye irritation upon contact. Certain individuals may also develop an allergic reaction after exposure (skin contact, inhalation of vapors, etc.) which may manifest itself in a number of ways including skin rashes and an itching sensation. Handling this product at elevated temperatures may also generate vapors irritating to the respiratory system.

Good industrial hygiene and safety practices should be followed when handling this product. Proper eye protection and appropriate chemical resistant clothing should be worn to minimize direct contact. Consult the Material Safety Data Sheet (MSDS) for detailed recommendations on the use of engineering controls and personal protective equipment.

This information is only a brief summary of the available safety and health data. Thoroughly review the MSDS for more complete information before using this product.

Attention Specification Writers:

The values contained herein are considered typical properties only and are not intended to be used as specification limits. For assistance in preparing specifications, please contact Emerson & Cuming Quality Assurance for further details.

APPENDIX B

EES MODEL SOURCE CODE

Case #1

          NASA GODDARD SPACE FLIGHT CENTER - CRYOGENICS AND FLUID BRANCH
          UNIVERSITY OF PUERTO RICO - DEPARTMENT OF MECHANICAL ENGINEERING

   XRS HTCS LEADS HEAT LOAD CALCULATION MODEL

   THIS CODE CALCULATE THE HEAT LOAD THROUGH A SINGLE WIRE WITH VARIABLE CONDUCTIVITY

   WRITE BY VICTOR L. MARRERO
   REVISED BY JOHN PANEK, PhD
   DECEMBER, 2002
   ***"

```
"!*********************** SS316 CONDUCTIVITY CALCULATION ***************************"
FUNCTION K_ss(T_h,T_l)
SS_0=2.77792*10^(-5)
SS_1=6.5069*10^(-4)
SS_2=3.10766*10^(-5)
SS_3=-4.34032*10^(-7)
K_S:=SS_0*(T_h-T_l)+SS_1/2*(T_h^2-T_l^2)+SS_2/3*(T_h^3-T_l^3)+SS_3/4*(T_h^4-T_l^4)  "[W/cm]"
K_ss:=K_S/(T_h-T_l)  "[W/cm-K]"
END


"!********************** TEFLON CONDUCTIVITY CALCULATION ***************************"
FUNCTION K_tf(T_h,T_l)
TF_0=0.00016119
TF_1=0.000089238
TF_2=-1.4482*10^(-6)
TF_3=8.3371*10^(-9)
K_T:=TF_0*(T_h-T_l)+TF_1/2*(T_h^2-T_l^2)+TF_2/3*(T_h^3-T_l^3)+TF_3/4*(T_h^4-T_l^4)  "[W/cm]"
K_tf:=K_T/(T_h-T_l)  "[W/cm-K]"
END


"!***************************** CONSTANT VARIABLES ********************************"
dx_c=0.25*Convert(in,cm)                        "[cm] Delta-x Cold Side"
dx_w=0.25*Convert(in,cm)                        "[cm] Delta-x Warm Side"


L_w=5.5                                         "[in]  Warm Side  Length"
L_c= 3.5                                        "[in]  Cold Side Length"
L_t=L_w+L_c                                     "[in]  HTC Total Length"


pts_c=L_c*Convert(in,cm)/dx_c                   "Number of Cold Points"
pts_w=1+L_w*Convert(in,cm)/dx_w                 "Number of Warm Points"
pts_t=pts_c+pts_w                               "Total Number of Points"


T[0]=18                                         "[K]  Warm End Temperature"
T[pts_t-1]=1.1                                  "[K]  Cold End Temperature"
Boltz=5.67*10^(-8)                              "[W/m^2-K^4] Boltzman Constant"
D_ss=0.015                                      "[in] Stainless Steel 316 Wire Diameter"
D_tf=0.034                                      "[in] Teflon Insulation Diameter"
Ar_c=PI*(D_tf*Convert(in,cm))*.25*dx_c          "[cm^2] Wire Radiation Area in the Cold Section"
Ar_w=PI*(D_tf*Convert(in,cm))*.75*dx_w          "[cm^2] Wire Radiation Area in the Warm Section"
Ac_ss=PI*(D_ss*Convert(in,cm)/2)^2              "[cm^2] SS316 Wire Conduction Area"
Ac_tf=PI*(D_tf*Convert(in,cm)/2)^2 - Ac_ss      "[cm^2] Teflon Insulation Conduction Area"

{e=1}                                           "Teflon Emissivity"

T_w=17.0                                         "[K] Radiation Shield Temperature"
T_c=1.3                                          "[K] Base Plate Temperature"
T[pts_w-1]=4                                     "[K] 4 K Heat Sink Temperature"
```

```
"!****************************** WARM SIDE ******************************"
DUPLICATE i=1,pts_w-1
Q_ss[i]=-1*(T[i]-T[i-1])*K_ss(T[i-1],T[i])*Ac_ss/dx_w          "[W]  Heat Conduction in SS316"
Q_tf[i]=-1*(T[i]-T[i-1])*K_tf(T[i-1],T[i])*Ac_tf/dx_w          "[W]  Heat Conduction in Teflon"
Q[i]=Q_ss[i]+Q_tf[i]                                           "[W]  Total Heat Conduction"
END

DUPLICATE j=1,pts_w-2
Q[j]+Qri[j]=Q[j+1]+Qro[j]
Qri[j]=e*Boltz*Convert(W/m^2-K^4,W/cm^2-K^4)*Ar_w*(T_w^4-T[j]^4)    "[W]  Radiation In"
Qro[j]=e*Boltz*Convert(W/m^2-K^4,W/cm^2-K^4)*Ar_w*(T[j]^4-T_c^4)    "[W]  Radiation Out"
END
"!****************************** WARM SIDE END ******************************"

Qri[pts_w-1]+Q[pts_w-1]=Q[pts_w]+Qro[pts_w-1]+Q_hsk                          "Energy Balance @ Heat Sink"
Qri[pts_w-1]=e*Boltz*Convert(W/m^2-K^4,W/cm^2-K^4)*Ar_w*(T_w^4-T[pts_w-1]^4)   "[W]  Radiation In @ Heat Sink"
Qro[pts_w-1]=e*Boltz*Convert(W/m^2-K^4,W/cm^2-K^4)*Ar_c*(T[pts_w-1]^4-T_c^4)   "[W] Radiation Out @ Heat Sink"


"!****************************** COLD SIDE ******************************"
DUPLICATE i=pts_w,pts_t-1
Q_ss[i]=-1*(T[i]-T[i-1])*K_ss(T[i-1],T[i])*Ac_ss/dx_c          "[W]  Heat Conduction in SS316"
Q_tf[i]=-1*(T[i]-T[i-1])*K_tf(T[i-1],T[i])*Ac_tf/dx_c          "[W]  Heat Conduction in Teflon"
Q[i]=Q_ss[i]+Q_tf[i]                                           "[W]  Total Heat Conduction"
END

DUPLICATE j=pts_w,pts_t-2
Q[j]+Qri[j]=Q[j+1]+Qro[j]
Qri[j]=e*Boltz*Convert(W/m^2-K^4,W/cm^2-K^4)*Ar_c*(T_w^4-T[j]^4)    "[W]  Radiation In"
Qro[j]=e*Boltz*Convert(W/m^2-K^4,W/cm^2-K^4)*Ar_c*(T[j]^4-T_c^4)    "[W]  Radiation Out"
END
"!****************************** COLD SIDE END ******************************"

Q_Thsk=12*Q_hsk          "[W] Total Heat Going to the 4 K Heat Sink"
Q_C_end=12*Q[pts_t-2]    "[W] Total Heat Going to the 1.3 K End"
Q_T=Q_C_end+0.145*Q_Thsk "[W] Total Heat Going to the Cryostat"
```

Case #2

```
                    NASA GODDARD SPACE FLIGHT CENTER - CRYOGENICS AND FLUID BRANCH
                    UNIVERSITY OF PUERTO RICO - DEPARTMENT OF MECHANICAL ENGINEERING

    XRS HTCS LEADS HEAT LOAD CALCULATION MODEL

    THIS CODE CALCULATE THE HEAT LOAD THROUGH A SINGLE WIRE WITH VARIABLE CONDUCTIVITY

    WRITE BY VICTOR L. MARRERO
    REVISED BY SANDRA COUTIN, PhD
    DECEMBER, 2003
"!****************************************************************************************************"


"!*********************** MgB2 CONDUCTIVITY CALCULATION ****************************"
FUNCTION K_MgB(T_h,T_l)
MgB_0=-0.0014
MgB_1=0.0027
MgB_2=0.0004
MgB_3=-6*10^(-6)
K_Mg:=MgB_0*(T_h-T_l)+MgB_1/2*(T_h^2-T_l^2)+MgB_2/3*(T_h^3-T_l^3)+MgB_3/4*(T_h^4-T_l^4)  "[W/cm]"
K_MgB:=K_Mg/(T_h-T_l)  "[W/cm-K]"
END


"!********************** TEFLON CONDUCTIVITY CALCULATION ***************************"
FUNCTION K_tf(T_h,T_l)
TF_0=0.00016119
TF_1=0.000089238
TF_2=-1.4482*10^(-6)
TF_3=8.3371*10^(-9)
K_T:=TF_0*(T_h-T_l)+TF_1/2*(T_h^2-T_l^2)+TF_2/3*(T_h^3-T_l^3)+TF_3/4*(T_h^4-T_l^4)  "[W/cm]"
K_tf:=K_T/(T_h-T_l)  "[W/cm-K]"
END


"!****************************** CONSTANT VARIABLES *********************************"
dx_c=0.25*Convert(in,cm)                        "[cm] Delta-x Cold Side"
dx_w=0.25*Convert(in,cm)                        "[cm] Delta-x Warm Side"

L_w=5.5                                         "[in]  Warm Side  Length"
L_c= 3.5                                        "[in]  Cold Side Length"
L_t=L_w+L_c                                     "[in]  HTC Total Length"


pts_c=L_c*Convert(in,cm)/dx_c                   "Number of Cold Points"
pts_w=1+L_w*Convert(in,cm)/dx_w                 "Number of Warm Points"
pts_t=pts_c+pts_w                               "Total Number of Points"

T[0]=18                                         "[K]  Warm End Temperature"
T[pts_t-1]=1.1                                  "[K]  Cold End Temperature"
Boltz=5.67*10^(-8)                              "[W/m^2-K^4] Boltzman Constant"
D_MgB=0.015                                     "[in] MgB2 Wire Diameter"
D_tf=0.034                                      "[in]  Teflon Insulation Diameter"
Ar_c=PI*(D_tf*Convert(in,cm))*.25*dx_c          "[cm^2]  Wire Radiation Area in the Cold Section"
Ar_w=PI*(D_tf*Convert(in,cm))*.75*dx_w          "[cm^2]  Wire Radiation Area in the Warm Section"
Ac_MgB=PI*(D_MgB*Convert(in,cm)/2)^2            "[cm^2] MgB2 Wire Conduction Area"
Ac_tf=PI*(D_tf*Convert(in,cm)/2)^2 - Ac_MgB     "[cm^2]  Teflon Insulation Conduction Area"

{e=1}                                           "Teflon Emissivity"

T_w=17.0                                        "[K] Radiation Shield Temperature"
T_c=1.3                                         "[K] Base Plate Temperature"
T[pts_w-1]=4                                    "[K] 4 K Heat Sink Temperature"
```

```
"!******************************  WARM SIDE  ******************************"
DUPLICATE i=1,pts_w-1
Q_MgB[i]=-1*(T[i]-T[i-1])*K_MgB(T[i-1],T[i])*Ac_ss/dx_w          "[W]  Heat Conduction in MgB2"
Q_tf[i]=-1*(T[i]-T[i-1])*K_tf(T[i-1],T[i])*Ac_tf/dx_w            "[W]  Heat Conduction in Teflon"
Q[i]=Q_MgB[i]+Q_tf[i]                                            "[W]  Total Heat Conduction"
END

DUPLICATE j=1,pts_w-2
Q[j]+Qri[j]=Q[j+1]+Qro[j]
Qri[j]=e*Boltz*Convert(W/m^2-K^4,W/cm^2-K^4)*Ar_w*(T_w^4-T[j]^4)   "[W]  Radiation In"
Qro[j]=e*Boltz*Convert(W/m^2-K^4,W/cm^2-K^4)*Ar_w*(T[j]^4-T_c^4)   "[W]  Radiation Out"
END
"!******************************  WARM SIDE END  ******************************"

Qri[pts_w-1]+Q[pts_w-1]=Q[pts_w]+Qro[pts_w-1]+Q_hsk                            "Energy Balance @ Heat Sink"
Qri[pts_w-1]=e*Boltz*Convert(W/m^2-K^4,W/cm^2-K^4)*Ar_w*(T_w^4-T[pts_w-1]^4)   "[W]  Radiation In @ Heat Sink"
Qro[pts_w-1]=e*Boltz*Convert(W/m^2-K^4,W/cm^2-K^4)*Ar_c*(T[pts_w-1]^4-T_c^4)   "[W]  Radiation Out @ Heat
Sink"


"!******************************  COLD SIDE  ******************************"
DUPLICATE i=pts_w,pts_t-1
Q_MgB[i]=-1*(T[i]-T[i-1])*K_ss(T[i-1],T[i])*Ac_ss/dx_c          "[W]  Heat Conduction in MgB2"
Q_tf[i]=-1*(T[i]-T[i-1])*K_tf(T[i-1],T[i])*Ac_tf/dx_c           "[W]  Heat Conduction in Teflon"
Q[i]=Q_MgB[i]+Q_tf[i]                                           "[W]  Total Heat Conduction"
END

DUPLICATE j=pts_w,pts_t-2
Q[j]+Qri[j]=Q[j+1]+Qro[j]
Qri[j]=e*Boltz*Convert(W/m^2-K^4,W/cm^2-K^4)*Ar_c*(T_w^4-T[j]^4)   "[W]  Radiation In"
Qro[j]=e*Boltz*Convert(W/m^2-K^4,W/cm^2-K^4)*Ar_c*(T[j]^4-T_c^4)   "[W]  Radiation Out"
END
"!******************************  COLD SIDE END  ******************************"

Q_Thsk=12*Q_hsk           "[W] Total Heat Going to the 4 K Heat Sink"
Q_C_end=12*Q[pts_t-2]     "[W] Total Heat Going to the 1.3 K End"
Q_T=Q_C_end+0.145*Q_Thsk  "[W] Total Heat Going to the Cryostat"
```

Case #3

```
"!*******************************************************************************************************"
              NASA GODDARD SPACE FLIGHT CENTER - CRYOGENICS AND FLUID BRANCH
              UNIVERSITY OF PUERTO RICO - DEPARTMENT OF MECHANICAL ENGINEERING

   XRS HTCS LEADS HEAT LOAD CALCULATION MODEL

   THIS CODE CALCULATE THE HEAT LOAD THROUGH A SINGLE WIRE WITH VARIABLE CONDUCTIVITY

   WRITE BY VICTOR L. MARRERO
   REVISED BY SANDRA COUTIN, PhD
   DECEMBER, 2003
"!*******************************************************************************************************"


"!************************* MgB2 CONDUCTIVITY CALCULATION  ***************************"
FUNCTION K_MgB(T_h,T_l)
MgB_0=-0.0014
MgB_1=0.0027
MgB_2=0.0004
MgB_3=-6*10^(-6)
K_Mg:=MgB_0*(T_h-T_l)+MgB_1/2*(T_h^2-T_l^2)+MgB_2/3*(T_h^3-T_l^3)+MgB_3/4*(T_h^4-T_l^4)  "[W/cm]"
K_MgB:=K_Mg/(T_h-T_l)  "[W/cm-K]"
END

"!********************** TEFLON CONDUCTIVITY CALCULATION  ***************************"
FUNCTION K_tf(T_h,T_l)
TF_0=0.00016119
TF_1=0.000089238
TF_2=-1.4482*10^(-6)
TF_3=8.3371*10^(-9)
K_T:=TF_0*(T_h-T_l)+TF_1/2*(T_h^2-T_l^2)+TF_2/3*(T_h^3-T_l^3)+TF_3/4*(T_h^4-T_l^4)  "[W/cm]"
K_tf:=K_T/(T_h-T_l)  "[W/cm-K]"
END

"!*************************** CONSTANT VARIABLES  ******************************"
dx_c=0.25*Convert(in,cm)                        "[cm] Delta-x Cold Side "
dx_w=0.25*Convert(in,cm)                        "[cm] Delta-x Warm Side "
dx_wc=0.25*Convert(in,cm)                       "[cm] Delta-x Warm-Cold Side "

L_w=7                                           "[in]  Warm Side  Length"
L_c= 1                                          "[in]  Cold Side Length"
L_wc=1                                          "[in]  Warm-Cold Side Length"
L_t=L_w+L_c+L_wc                                "[in]  HTC Total Length"


pts_c=L_c*Convert(in,cm)/dx_c                   "Number of Cold Points"
pts_w=1+L_w*Convert(in,cm)/dx_w                 "Number of Warm Points"
pts_wc=L_wc*Convert(in,cm)/dx_wc                "Number of Warm Points"
pts_t=pts_c+pts_w+pts_wc                        "Total Number of Points"


T[0]=17                                         "[K]  Warm End Temperature"
T[pts_t-1]=1.3                                  "[K]  Cold End Temperature"
Boltz=5.67*10^(-8)                              "[W/m^2-K^4] Stefan-Boltzman Constant"
D_MgB=0.015                                     "[in]  MgB2 Wire Diameter"
D_tf=0.034                                      "[in]  Teflon Insulation Diameter"
Ar_c=PI*(D_tf*Convert(in,cm))*.25*dx_c          "[cm^2]  Wire Radiation Area in the Cold Section"
Ar_w=PI*(D_tf*Convert(in,cm))*.75*dx_w          "[cm^2]  Wire Radiation Area in the Warm Section"
Ac_MgB=PI*(D_MgB*Convert(in,cm)/2)^2            "[cm^2]  MgB2 Wire Conduction Area"
Ac_tf=PI*(D_tf*Convert(in,cm)/2)^2 - Ac_MgB     "[cm^2]  Teflon Insulation Conduction Area"

{e=1}                                           "Teflon Emissivity"

pts_w_c=(pts_w+pts_wc)
```

91

```
T_w=17.0                                        "[K] Radiation Shield Temperature"
T_c=1.3                                         "[K] Base Plate Temperature"
T[pts_w-1]=10                                   "[K] 10 K Heat Sink Temperature"
T[pts_w-1]=4                                    "[K] 4 K Heat Sink Temperature"


"!******************************** WARM SIDE **************************************"
DUPLICATE i=1,pts_w-1
Q_MgB[i]=-1*(T[i]-T[i-1])*K_MgB(T[i-1],T[i])*Ac_MgB/dx_w        "[W] Heat Conduction in MgB2"
Q_tf[i]=-1*(T[i]-T[i-1])*K_tf(T[i-1],T[i])*Ac_tf/dx_w          "[W] Heat Conduction in Teflon"
Q[i]=Q_MgB[i]+Q_tf[i]                                          "[W] Total Heat Conduction"
END


DUPLICATE j=1,pts_w-2
Q[j]+Qri[j]=Q[j+1]+Qro[j]
Qri[j]=e*Boltz*Convert(W/m^2-K^4,W/cm^2-K^4)*Ar_w*(T_w^4-T[j]^4)    "[W] Radiation In"
Qro[j]=e*Boltz*Convert(W/m^2-K^4,W/cm^2-K^4)*Ar_w*(T[j]^4-T_c^4)    "[W] Radiation Out"
END
"!******************************** WARM SIDE END **************************************"

Qri[pts_w-1]+Q[pts_w-1]=Q[pts_w]+Qro[pts_w-1]+Q_hsk10                "Energy Balance @ Heat Sink"
Qri[pts_w-1]=e*Boltz*Convert(W/m^2-K^4,W/cm^2-K^4)*Ar_w*(T_w^4-T[pts_w-1]^4)    "[W] Radiation In @ Heat Sink"
Qro[pts_w-1]=e*Boltz*Convert(W/m^2-K^4,W/cm^2-K^4)*Ar_wc*(T[pts_w_c-1]^4-T_c^4)    "[W] Radiation Out @ Heat
Sink"


"!******************************** WARM-COLD SIDE **************************************"
DUPLICATE i=pts_w,pts_w_c-1
Q_MgB[i]=-1*(T[i]-T[i-1])*K_MgB(T[i-1],T[i])*Ac_MgB/dx_wc       "[W] Heat Conduction in MgB2"
Q_tf[i]=-1*(T[i]-T[i-1])*K_tf(T[i-1],T[i])*Ac_tf/dx_wc          "[W] Heat Conduction in Teflon"
Q[i]=Q_MgB[i]+Q_tf[i]                                          "[W] Total Heat Conduction"
END


DUPLICATE j=pts_w,pts_w_c-2
Q[j]+Qri[j]=Q[j+1]+Qro[j]
Qri[j]=e*Boltz*Convert(W/m^2-K^4,W/cm^2-K^4)*Ar_wc*(T_w^4-T[j]^4)    "[W] Radiation In"
Qro[j]=e*Boltz*Convert(W/m^2-K^4,W/cm^2-K^4)*Ar_wc*(T[j]^4-T_c^4)    "[W] Radiation Out"
END
"!******************************** WARM-COLD SIDE END **************************************"

Qri[pts_w-1]+Q[pts_w_c-1]=Q[pts_w]+Qro[pts_w_c-1]+Q_hsk                "Energy Balance @ Heat Sink"
Qri[pts_w-1]=e*Boltz*Convert(W/m^2-K^4,W/cm^2-K^4)*Ar_w*(T_w^4-T[pts_w_c-1]^4)    "[W] Radiation In @ Heat Sink"
Qro[pts_w-1]=e*Boltz*Convert(W/m^2-K^4,W/cm^2-K^4)*Ar_c*(T[pts_w_c-1]^4-T_c^4)    "[W] Radiation Out @ Heat
Sink"


"!******************************** COLD SIDE **************************************"
DUPLICATE i=pts_w_c,pts_t-1
Q_MgB[i]=-1*(T[i]-T[i-1])*K_MgB(T[i-1],T[i])*Ac_MgB/dx_c        "[W] Heat Conduction in MgB2"
Q_tf[i]=-1*(T[i]-T[i-1])*K_tf(T[i-1],T[i])*Ac_tf/dx_c          "[W] Heat Conduction in Teflon"
Q[i]=Q_MgB[i]+Q_tf[i]                                          "[W] Total Heat Conduction"
END


DUPLICATE j=pts_w_c,pts_t-2
Q[j]+Qri[j]=Q[j+1]+Qro[j]
Qri[j]=e*Boltz*Convert(W/m^2-K^4,W/cm^2-K^4)*Ar_c*(T_w^4-T[j]^4)    "[W] Radiation In"
Qro[j]=e*Boltz*Convert(W/m^2-K^4,W/cm^2-K^4)*Ar_c*(T[j]^4-T_c^4)    "[W] Radiation Out"
END
"!******************************** COLD SIDE END **************************************"

Q_Thsk10=12*Q_hsk10                             "[W] Total Heat Going to the 10 K Heat Sink"
Q_Thsk4=12*Q_hsk4                               "[W] Total Heat Going to the 4 K Heat Sink"
Q_C_end=12*Q[pts_t-2]                           "[W] Total Heat Going to the 1.3 K End"
Q_T=Q_C_end+0.0714*Q_Thsk4+0.01*Q_Thsk10        "[W] Total Heat Going to the Cryostat"
```